Mathematical Biosciences 390 (2025) 109540

Contents lists available at ScienceDirect

Mathematical Biosciences

journal homepage: www.elsevier.com/locate/mbs

Original Research Article

Natural population dynamics of Asian citrus psyllid, *Diaphorina citri*, and its control based on pheromone trapping

Daiver Cardona-Salgado [a], Yves Dumont [b,c,d], Olga Vasilieva [e,*]

[a] Department of Mathematics, Universidad Autonoma de Occidente, Cali, 760032, Colombia
[b] CIRAD, UMR AMAP, Pole de Protection des Plantes, Saint-Pierre, F-97410, Reunion island, France
[c] AMAP, University of Montpellier, CIRAD, CNRS, INRAE, IRD, Montpellier, 34090, France
[d] Department of Mathematics and Applied Mathematics, University of Pretoria, Pretoria, 001, South Africa
[e] Department of Mathematics, Universidad del Valle, Cali, 760031, Colombia

ARTICLE INFO

MSC:
92D25
92D45
37N25

Keywords:
Diaphorina citri
Asian citrus psyllid
Pheromone traps
Mating disruption
Piecewise smooth system
Local stability
Open- and closed-loop control

ABSTRACT

The Asian citrus psyllid (*Diaphorina citri*) is a major agricultural pest and the principal vector of Huanglongbing (HLB), a devastating citrus disease. Thus, its control is of utmost importance: since *D. citri* mates multiple times, the use of mating disruption has the potential to reduce or eliminate populations. In this work, we develop a sex-structured, piecewise smooth dynamical system modeling the natural population dynamics of *D. citri*, focusing on adult stages and mating behavior. The main goal of this manuscript is to show that the population of *D. citri*, when near a locally asymptotically stable equilibrium, can be effectively suppressed using pheromone traps via two control strategies, mating disruption and male-targeted removal. For this reason, we focus on local stability analysis and the design of practical control interventions that are biologically meaningful and implementable. By applying a feed-forward control approach, which only requires assessing the initial size of the psyllid population, we identify the threshold as a function of the two control parameters above which a local insect elimination is reachable. We also show that a feedback control with periodic assessments of the wild population sizes is applicable, and then deduce that a mixed-type control regime, combining both studied control approaches, yields the best results. We present several simulations to illustrate our theoretical findings and to estimate the minimal amount of pheromones and time needed to reach the local elimination of existing psyllids. Finally, we discuss possible implementations of our results as a part of Integrated Pest Management programs.

1. Introduction

The Asian citrus psyllid (ACP) [1,2], *Diaphorina citri* Kuwayama (Hemiptera: Liviidae), is the most important pest of citrus cultures because it is the main vector of *Candidatus* Liberibacter spp., the bacterium that cause Huanglongbing (HLB), the citrus greening disease [3], impacting several places around the world, and, in particular, Colombia [4] and also La Réunion, a French overseas department. When uninfected psyllids feed on an infected citrus tree, they acquire the bacterium. Subsequently, when they feed on healthy trees, they can transmit the bacterium, thereby spreading the disease. Note also that in La Réunion another psyllid, the African citrus psyllid, *Trioza erytreae*, has been identified as an efficient vector of *Candidatus* Liberibacter asiaticus [5]. Since there is no cure for infected trees, several control strategies have been developed, including the removal and destruction of infected trees to prevent further spread, the use of insecticides to control the population of psyllid, quarantine measures to limit the movement of infected plant material, research into disease-resistant citrus varieties through breeding programs, development of early detection methods to identify infected trees, etc. So far, only in La Réunion the biological HBL control was achieved successfully in the late 1970s [6].

D. citri started to be reported in the Caribbean basin in the late 1990s [7], before being first officially reported in Colombia in 2007 [8,9]. While single insecticides and insecticide rotations have also been tested against *D. citri* [9], the biological control of *D. citri* has been pursued through several complementary strategies. Among the most effective methods, the use of the natural predators and parasitoids (especially *Tamarixia radiata*) rendered noticeable results for population suppression in multiple regions [6,8,10–12]. Entomopathogenic fungi have also shown promise, causing significant psyllid mortality in both laboratory and field settings [13,14]. More recently, attention

* Corresponding author.
E-mail address: olga.vasilieva@correounivalle.edu.co (O. Vasilieva).

https://doi.org/10.1016/j.mbs.2025.109540
Received 18 November 2024; Received in revised form 9 June 2025; Accepted 17 September 2025
Available online 3 October 2025

has turned to semiochemical-based methods [15,16], such as the use of female-emitted sex pheromones to attract males for mating disruption and direct trapping. The pheromone-based approach is environmentally friendly and species-specific, offering a promising alternative (or complement) to chemical insecticides within Integrated Pest Management programs (IPMs).

However, finding or synthesizing an efficient pheromone compound can be a long, challenging, and tedious task because sex pheromones are specific to each pest. A recent review [17] summarizes the existing pheromone-based techniques for controlling other different pests, while in Brazil, the ACP biological control with sex pheromones [18,19] is under study. In the present work, we address the pheromone-based control of *D. citri* from the standpoint of mathematical modeling.

Mathematical modeling is now a common tool to study (biological) control strategies against pests [20] and vectors [21]. In particular, several models have been developed and studied to control the spreading of HLB: see [22] for an overview and references therein. The majority of these models are epidemiological models based on vector-borne disease models developed for mosquitoes. In [23], the authors developed an ACP continuous population model to study the effect of physiological and behavioral resistance and investigate the existence of threshold conditions for extinction. Discrete ACP models for each stage (eggs, nymphs, and adults) have been developed in [24] to study the impact of environmental parameters, habitat, and natural enemies on the ACP dynamics in an urban area in California. However, these phenological models are degree-day models, i.e., based on a temperature accumulation, and thus well adapted to study population accumulation of *D. citri* and the effect of temperature.

Several multi-compartment models were also proposed to characterize the spread of HLB in orchards and evaluate the impact of vector management interventions. These models typically couple host plant and vector dynamics, integrating epidemiological compartments for both the host and the vector [25–27]. However, these models share the same drawback: they oversimplify the ACP population dynamics by assuming a logistic-type approach, and thus ignoring the psyllid's mating behavior entirely. In this paper, we employ a piecewise smooth modeling approach to investigate the impact of sex pheromone emissions on the mating disruption of psyllids.

Our study has benefited from the results of previous works [20,21,28] featuring mating disruption and adapted to other insect populations different from *D. citri*. However, the models proposed and analyzed in [20,21,28] exhibit stage structure that leads to the property of monotonicity of the dynamical system describing them. In contrast, the model presented in this study is non-monotone, and its analysis cannot benefit from the properties usually exhibited by monotone systems. Moreover, the analysis of our model is carried out using biological characteristics of the insect populations, such as basic offspring numbers corresponding to male and female insects, denoted in the sequel by $\mathcal{N}_M$ and $\mathcal{N}_F$, respectively. As the quantities $\mathcal{N}_M$ and $\mathcal{N}_F$ characterize the reproduction rate of male and female insects, the relationships between them define the evolution of the sex-structured adult psyllid population described by a piecewise smooth dynamical system, which is another highlight of our model.

Furthermore, our model describing the natural ACP population dynamics is amended with two control parameters related to pheromone emissions through male-killing traps, which are part of the so-called Integrated Pest Management (IPM) programs. Using such a modification, we aim to prove the feasibility of pheromone-based control under certain conditions, which must be considered before trying to implement this type of pest control in practice. In other words, we intend to show that a local APC population can be eliminated (or at least suppressed) when certain conditions imposed on the pheromone traps are met. Even though we do not estimate direct monetary costs related to using pheromone traps, our study reveals some essential tradeoffs that provide helpful ideas for implementing this type of pest control.

When studying the impact of pheromone emissions through male-killing traps on the suppression and possible elimination of the ACP populations, we consider two approaches. One is known as "open-loop control" and operates on a predefined sequel of actions. It does not require an assessment of the current size of the pest population. Another is called "closed-loop control", whose actions are defined depending on the current size of the pest population. Moreover, we also illustrate that combining the two approaches may have practical value. This is another difference of our study from the works [20,21] where only an open-loop control approach was proposed and evaluated.

The outline of the paper is as follows. In Section 2, we propose a sex-structured mathematical model that encompasses only the population of adult psyllids. The model is formulated as a piecewise smooth dynamical system in continuous time. In Section 3, dedicated to the qualitative analysis of the proposed model, the evolution of the natural ACP population dynamics is studied, and the underlying local stability properties of the piecewise smooth dynamical system are established. It is important to emphasize that our study is focused on the system's behavior near its unique locally stable equilibrium, while other complex analytical aspects (such as global stability or existence of other attracting set for specific parameter regimes, possible bifurcation, parameter sensitivity) related to the structural richness of piece-wise smooth dynamics, as these issues merit dedicated attention and cab be addressed in future studies. The proposed model is further amended in Section 4 with external control actions of pheromone traps: attraction and direct removal of male insects that induce mating disruption, targeting to reduce the future offspring. Assuming that the ACP population is near its locally stable positive equilibrium, these intervention measures are modeled by two control parameters, the male-killing rate and the strength of lure. The choice of these two parameters may result in two outcomes: the suppression or elimination of the local ACP population. To reach one of these goals, the open-loop and closed-loop operational control modes are suggested and validated in Section 4.1 and Section 4.2, respectively. Section 5 provides numerical simulations illustrating the open-loop and closed-loop control approaches. Finally, Section 6 summarizes the main results of our work.

2. Natural population dynamics of *Diaphorina citri*

D. citri are small (2.7 to 3.3 mm long) jumping and flying insects that live on citrus trees and feed on young stems, sprouts, and leaves during all stages of development. Their life cycle includes an immature phase (consisting of the egg stage and five nymphal instars) followed by the adult stage (imago) of sexually matured insects, males or females. Oviposition and development of immature *D. citri* elapse on young, tender flush leaves where the nymphs remain almost docile while feeding on the tissue of young leaves and stems until turning into adults [29].

In this section, we propose a sex-structured mathematical model that encompasses only the population of adult ACP, *D. citri*, even though the psyllid life cycle also includes the immature phase. Considering only the adult population of psyllids, our model has only three state variables, one less than the models studied in [20,21,28]. The latter allows readers to visualize the ACP population dynamics more clearly, making them more understandable for practitioners without advanced mathematical backgrounds, and also in the absence of information or data regarding the non-adult stages. Our model has been developed to mimic the particular ACP mating behavior, and only adult psyllids participate in this process. Thus, by not including explicitly the immature states, we achieve reduced dimensionality in the model, which makes it more comprehensible and straightforward. The model is based on the behavioral and biological features of this insect species, with particular attention paid to the ACP mating behavior.

Notably, our model has been designed by merging two modeling approaches. First, we have used as a basis the two-dimensional sex-structured model of Ricker type initially developed in [30] for

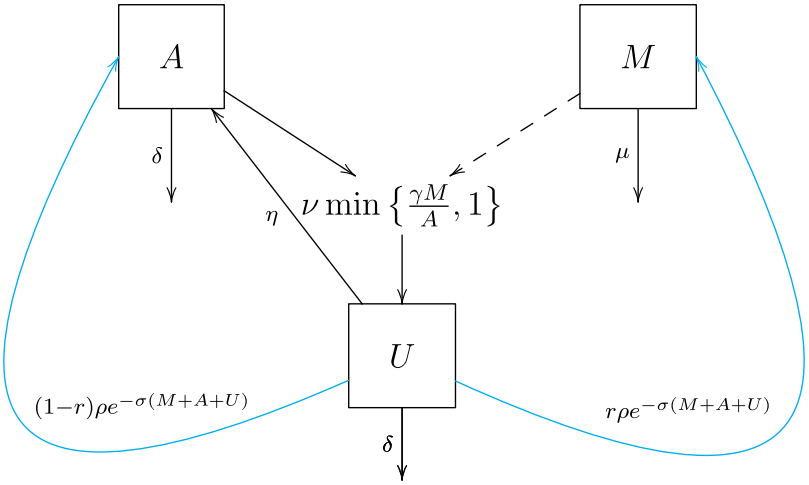

Fig. 1. Flow diagram of the natural ACP dynamics described by system (1).

mimicking the population dynamics of any pest or disease vector population. Second, as the female psyllids must remate after each oviposition to enhance fertility and continue laying viable eggs [31,32], we have introduced a separate female class gathering all female psyllids available for mating to mimic this particular mating process and following the approach developed in [20,21] while also employing the concept of mating function attributed to [33].

In fact, oviposition can also be reduced by the continuous presence of males seeking matings since this particular species (*D. citri*) exhibits a male-biased operational sex ratio [34], meaning that there are more sexually active males than sexually receptive females. Laboratory and field observations show that fertilized female psyllids become temporarily unavailable for mating and try to avoid males when they are ready for oviposition [35]. After oviposition, such female insects again exhibit receptiveness for mating. Thus, the female psyllids usually mate intermittently during their lives to keep an adequate amount of viable sperm and be able to lay eggs throughout their lives whenever young leaves and stems are present.

Insect populations in tropical regions that exhibit minimal or absent seasonal climate variations usually overlap. The latter implies that at each moment $t \geq 0$, certain amounts of living insects may bear diverse ages, including immature and adult stages. We will use the continuous-time Ricker-type model [30] amended with a particular ACP mating pattern to describe the evolution of well-mixed overlapping populations of the adult psyllids.

To mimic the ACP mating behavior, we divide the total population of adult psyllids into three disjoint compartments or population classes, namely:

- $M(t)$ – the number or density of male insects at the moment t.
- $A(t)$ – the number or density of female insects available for mating at the moment t.
- $U(t)$ – the number or density of fertilized female insects at the moment t (they avoid mating while preparing for oviposition).

Thus, $F(t) := A(t) + U(t)$ constitutes the total population of female psyllids. It is also supposed that all male insects $M(t)$ are available for mating anytime and remain sexually active during their lifetime.

Following the approach of [20,21], and according to the flow diagram provided in Fig. 1, we derive the following dynamical system to describe the population dynamics of adult psyllids

$$\begin{cases} \dfrac{dM}{dt} = r\rho U e^{-\sigma(M+A+U)} - \mu M, & \text{(1a)} \\ \dfrac{dA}{dt} = (1-r)\rho U e^{-\sigma(M+A+U)} - \nu \min\left\{\dfrac{\gamma M}{A}, 1\right\} A + \eta U - \delta A, & \text{(1b)} \\ \dfrac{dU}{dt} = \nu \min\left\{\dfrac{\gamma M}{A}, 1\right\} A - \eta U - \delta U, & \text{(1c)} \end{cases}$$

with nonnegative initial conditions

$$M(0) = M_0, \quad A(0) = A_0, \quad U(0) = U_0. \tag{2}$$

In what follows, we will deal only with nonnegative solutions of the system (1)–(2) to preserve its biological meaningfulness, and also prove that any solution $\big(M(t), A(t), U(t)\big)$ of the system (1) engendered by $\big(M_0, A_0, U_0\big) \in \mathbb{R}^3_+$ will remain nonnegative for all $t \geq 0$.

The constant parameters included in the model (1) are all positive, and their concise definitions, as well as numerical values in simulations (Section 5), are summarized in Table 1. Notably, these parameter values are borrowed from a field study [36] on Valencia sweet orange tree (*Citrus sinensis*) with Rangpur lime (*Citrus limonia*) as a rootstock; however, further experimental studies might be needed to refine these estimates.

In the Eqs. (1a) and (1b), we denote by r and $(1-r)$ with $r \in (0,1)$ the proportion of male and female psyllids emerging from the immature stage and entering the compartments of males and receptive females, respectively.

The parameter $\rho > 0$ stands for the mean number of eggs produced on average per day by one female psyllid from the class U. At the same time, the exponential factor in the recruitment terms of Eqs. (1a) and (1b) expresses the eggs' survival to adulthood while they pass through five nymphal instars. Notably, this factor does not involve the time scale because the populations M and $F = A+U$ are supposed to overlap, meaning that each population group M, A, and U is well-mixed and contains individuals of different ages.

The exponential factor, $e^{\sigma(M+A+U)}$, in the birth rates of male and female psyllids (see Eqs. (1a), (1b)) is inherent from Ricker-type population dynamics models [30] and it helps mimic the density-dependent population growth. Here, the parameter $\sigma > 0$ may be seen as the ratio $\sigma = \beta/K$ between β, a quantity characterizing the transition of immature insects into adults under density dependence and nymphal competition for food resources, and a carrying capacity K. The latter is typically proportional to the capacity of available breeding sites (young stems, sprouts, and leaves) that also provide food for all nymphal stages and adults (males and two classes of females). Thus, our model implicitly takes into account the environmental carrying capacity through

Table 1
Parameters of the model (1) with some values corresponding to the field study performed on Valencia sweet orange tree (*Citrus sinensis*) with Rangpur lime (*Citrus limonia*) taken as a rootstock.

Parameter	Description	Value	Unit	References
r	primary sex ratio	0.41	–	[36]
ρ	mean no. of eggs produced by one female per day	6.352	day^{-1}	[36]
σ	characteristic of eggs survival to the adult stage	0.001	individual^{-1}	assumed
μ	natural mortality rate for males	0.021	day^{-1}	[36]
δ	natural mortality rate for females	0.023	day^{-1}	[36]
γ	females fertilized by a single male	1.2	–	[36]
ν	transfer rate from A to U	1/4	day^{-1}	estimated from [19]
η	transfer rate from U to A	1	day^{-1}	[32]

the parameter σ, unlike the models considered in [20,21,28,37], all developed using the logistic-type modeling approach, which explicitly includes the carrying capacity of immature states, a parameter that is not easy to estimate.

Natural mortality rates for adult males M and females ($F = A + U$) are denoted by μ and δ, respectively, and correspond to the inverses of their average lifespans ($1/\mu$ and $1/\delta$ days, respectively). Some studies report that female psyllids live longer than males (see [29,36] and more detailed references therein), so we suppose in the sequel that $\mu \geq \delta$.

Further, we assume that a receptive female A needs to mate once or more to pass into the class U of eggs-laying females and be able to reproduce. The conversion of mating females A into eggs-laying females U is modeled using the so-called mating function $\min\left\{\frac{\gamma M}{A}, 1\right\}$ that appears in Eqs. (1b) and (1c). This function was proposed initially by Barclay & van den Driessche [33] for discrete-time models and further adapted to continuous-time models by Anguelov et al. [21] (see also [20,28,37]). Let us briefly explain the essence of modeling through the mating function.

Field studies [31,36] evince that APC males can successfully mate more than once per day. In Eqs. (1b) and (1c), the parameter $\gamma \geq 1$ expresses the relative number of females a single male can fertilize on average per one day, while the parameter ν is the transition rate of females from the non-fertilized compartment A to the fertilized class U. In other words, it is assumed that a sexually mature female becomes ready for oviposition after $1/\nu$ days from exhibiting receptiveness and completing at least one mating. The transition rate ν is weighted by the proportion of matings that depends on the current number of males related to the current number of females: if there are enough males so all females from class A can mate at least once, that is, $\gamma M \geq A$, then all females become fertilized and enter the eggs-laying class U at the rate ν.

Otherwise, if male psyllids are scarce, that is $\gamma M < A$, then only a fraction of mate-seeking females A can mate successfully and pass into the eggs-laying class U for further reproduction. In such a case, the mating function is $\min\left\{\frac{\gamma M}{A}, 1\right\} = \frac{\gamma M}{A} < 1$, meaning that the recruitment of fertilized females U is proportional to number of females that mated successfully ($\nu\gamma M$), while there will be still some females from the class A that could not mate on the day t. We also assume that after completing the oviposition, a female psyllid becomes receptive to mating again after $1/\eta$ days, leaves the class U and moves back to A-class.

Furthermore, using the approach developed in [21], system (1) can be written in the form

$$\frac{d\mathbf{X}}{dt} = \mathbf{\Phi}(\mathbf{X}) := \begin{cases} \mathbf{\Phi}_1(\mathbf{X}) & \text{if} \quad \gamma M \geq A \\ \mathbf{\Phi}_2(\mathbf{X}) & \text{if} \quad \gamma M \leq A \end{cases}, \tag{3}$$

where $\mathbf{X} := (M, A, U) \in \mathbb{R}^3_+$ and

$$\mathbf{\Phi}_1(\mathbf{X}) = \begin{pmatrix} r\rho U e^{-\sigma(M+A+U)} - \mu M \\ (1-r)\rho U e^{-\sigma(M+A+U)} - \nu A + \eta U - \delta A \\ \nu A - \eta U - \delta U \end{pmatrix}, \tag{4}$$

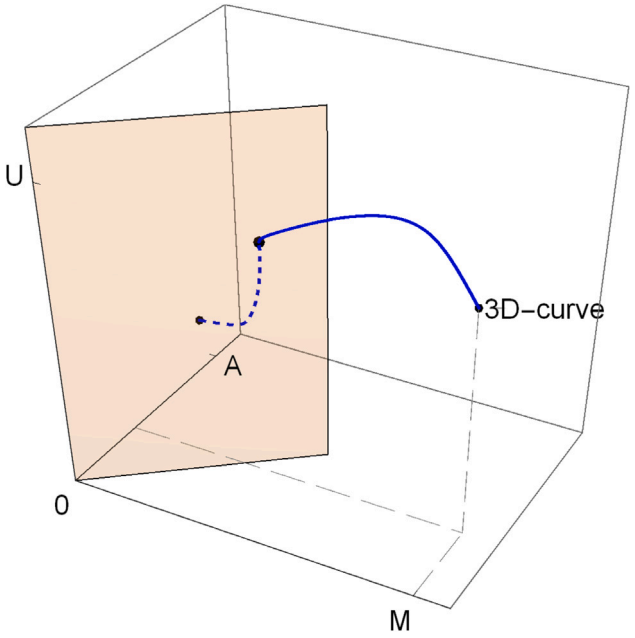

Fig. 2. A piecewise smooth solution $\big(M(t), A(t), U(t)\big)$ to the system (1) drawn as a parametric 3D-curve that crosses the switching plane $\mathcal{P}_s$ (shadowed area).

$$\mathbf{\Phi}_2(\mathbf{X}) = \begin{pmatrix} r\rho U e^{-\sigma(M+A+U)} - \mu M \\ (1-r)\rho U e^{-\sigma(M+A+U)} - \nu\gamma M + \eta U - \delta A \\ \nu\gamma M - \eta U - \delta U \end{pmatrix}. \tag{5}$$

Following definitions given in [38,39], the dynamical system defined by (1) or its equivalent form (3) can be considered as a *piecewise smooth (PWS) continuous* system with state-dependent switchings and the switching manifold defined by the plane

$$\mathcal{P}_s := \big\{(M, A, U) \in \mathbb{R}^3_+ : \ \gamma M = A\big\}$$

because any point $\tilde{\mathbf{X}} = (M, A, U) \in \mathcal{P}_s$ satisfies the relationship $\mathbf{\Phi}_1(\tilde{\mathbf{X}}) = \mathbf{\Phi}_2(\tilde{\mathbf{X}})$. Even though the first derivatives of $\mathbf{\Phi}$ in (3) have a jump discontinuity across the switching plane $\mathcal{P}_s$, their one-side limits are finite, and the jumps are bounded. Therefore, the overall vector field $\mathbf{\Phi}$ is autonomous, continuous, and piecewise smooth for all $\mathbf{X} = (M, A, U) \in \mathbb{R}^3_+$, the right-hand side of the dynamical system (3) is Lipschitz, and the states (M, A, U) do not jump when switchings occur. This not only guarantees the existence and uniqueness of a piecewise smooth solution to the initial-value problem (1)–(2) but also ensures that our PWS system (3) has the degree of smoothness equal to 2 (see more precise definitions in [21,39]) meaning that the trajectories of the system may only cross the switching plane $\mathcal{P}_s$ transversally and no sliding motion constrained to $\mathcal{P}_s$ can take place [38,39]. Fig. 2 gives an example of the piecewise smooth solution $\mathbf{X}(t) = \big(M(t), A(t), U(t)\big)$ to the system (1) in the form of a parametric 3D-curve that crosses the switching plane $\mathcal{P}_s$.

Let us denote by $\mathbf{X}(t; \mathbf{X}_0)$ the solution of (1) engendered by the initial condition $\mathbf{X}_0 := \big(M_0, A_0, U_0\big)$. If $\mathbf{X}_0 \in \mathbb{R}^3_+$ then it is easy to show that

$\mathbf{X}(t;\mathbf{X}_0) \in \mathbb{R}^3_+$. In effect, it is fulfilled that

$$\left.\frac{dM}{dt}\right|_{M=0} \geq 0, \qquad \left.\frac{dA}{dt}\right|_{A=0} \geq 0, \qquad \left.\frac{dU}{dt}\right|_{U=0} \geq 0.$$

Therefore, the positive invariance of $\mathbb{R}^3_+$ becomes obvious and we have $\mathbf{X}(t;\mathbf{X}_0) \geq 0$ for all $t \geq 0$ whenever $\mathbf{X}_0 \in \mathbb{R}^3_+$.

Furthermore, we can establish the following result related to the uniform ultimate boundedness of all solutions to the POS system (1).

Proposition 1. *There exists a compact absorbing set $\Omega \subset \mathbb{R}^3_+$ that attracts all the solutions of the PWS system (1) engendered by any initial condition $(M_0, A_0, U_0) \in \mathbb{R}^3_+$.*

Proof. First, we note that along the trajectories of (1), it is fulfilled that

$$\frac{d(M+A+U)}{dt} = \rho U e^{-\sigma(M+A+U)} - (\mu M + \delta A + \delta U) \leq (M+A+U)\Big[\rho e^{-\sigma(M+A+U)} - \min\{\mu,\delta\}\Big].$$

Therefore,

$$M(t) + A(t) + U(t) \leq \max\Big\{M_0 + A_0 + U_0, \widehat{P}\Big\},$$

where

$$\widehat{P} := \frac{1}{\sigma}\ln\left(\frac{\rho}{\min\{\mu,\delta\}}\right)$$

stands for the carrying capacity of the Ricker differential equation $P'(t) = P(t)\Big[\rho e^{-\sigma P(t)} - \min\{\mu,\delta\}\Big]$. Thus, the compact set

$$\Omega := \Big\{(M,A,U) \in \mathbb{R}^3_+ : \ 0 \leq M + A + U \leq \widehat{P}\Big\} \tag{6}$$

is invariant in the sense that any solution of (1) engendered by $(M_0, A_0, U_0) \in \Omega$ remains in Ω for all $t \geq 0$. Moreover, Ω attracts all the trajectories engendered by $(M_0, A_0, U_0) \in \mathbb{R}^3_+ \setminus \Omega$ and there is a finite time $\hat{t} > 0$ such that $(M(\hat{t}), A(\hat{t}), U(\hat{t})) \in \Omega$ for all $t \geq \hat{t}$. In other words, Ω constitutes the absorbing set of the PWS system (1), and its trajectories engendered by any initial condition $(M_0, A_0, U_0) \in \mathbb{R}^3_+$ are uniformly ultimately bounded. The existence of the absorbing set Ω also guarantees the global existence of the solution of the PWS system (3) for all $t \geq 0$. ■

Once the well-posedness of the PWS system (1) is formally established, we proceed to study its stability by applying the methodology employed in [20,21,28].

3. Qualitative analysis of the PWS system (1).

The switching plane $\mathcal{P}_s$ divides the positive octant $\mathbb{R}^3_+$ into two disjoint regions:

1. The *male abundance region*

   $$\mathbb{M}_a := \Big\{(M,A,U) \in \mathbb{R}^3_+ : \ \gamma M > A\Big\},$$

   where the vector field $\mathbf{\Phi}_1(\mathbf{X})$ defined by (4) takes action, that is,

   $$\frac{d\mathbf{X}}{dt} = \mathbf{\Phi}_1(\mathbf{X}). \tag{7}$$

2. The *male scarcity region*

   $$\mathbb{M}_s := \Big\{(M,A,U) \in \mathbb{R}^3_+ : \ \gamma M < A\Big\},$$

   where the vector field $\mathbf{\Phi}_2(\mathbf{X})$ defined by (5) takes action, that is,

   $$\frac{d\mathbf{X}}{dt} = \mathbf{\Phi}_2(\mathbf{X}). \tag{8}$$

As shown in Fig. 2, $\mathbb{M}_a$-region is in front of the switching plane $\mathcal{P}_s$ (shadowed area), whereas $\mathbb{M}_s$-region is behind $\mathcal{P}_s$. Both systems (7) and (8) have smooth right-hand sides. Their local stability properties can be studied separately, at least to understand better the overall dynamics of the original PWS system (1) whose behavior is richer and more complex than that of the two smooth ODE systems (7) and (8) when considered separately.

Generally speaking, a solution $\mathbf{X}(t;\mathbf{X}_0)$ with $\mathbf{X}_0 \in \mathbb{M}_s$ may remain in $\mathbb{M}_s$ or may enter the region $\mathbb{M}_a$ by crossing the switching plane $\mathcal{P}_s$ and then remain there (this situation is illustrated in Fig. 2). It is also not excluded that the mentioned solution leaves the region $\mathbb{M}_a$ and then returns or moves cyclically across the plane $\mathbb{P}_s$ (periodic or chaotic behavior). Similar behavior options also apply to solutions engendered by $\mathbf{X}_0 \in \mathbb{M}_a$. Therefore, for analyzing the behavior of solutions of the PWS system (3), the first step will be to identify the equilibria of (7) and (8) and then to study their stability properties separately. Further, we will explore their possible connections and relations with the equilibria of the PWS system (3).

It is worthwhile to recall that the PWS system (3) is continuous and exhibits only a constrained state-dependent switching. Additionally, the continuity of the vector field $\mathbf{\Phi}(\mathbf{X})$ defined by (3)–(5) ensures that any solution $\mathbf{X}(t;\mathbf{X}_0)$ with $\mathbf{X}_0 \in \mathbb{R}^3_+$ is continuously differentiable with respect to t. Based on [38,39], the trajectories of the PWS system (1) may only cross the switching plane $\mathcal{P}_s$ transversely, and no sliding motion constrained to $\mathcal{P}_s$ can take place. Moreover, according to [40], in such a case, the fundamental properties of each subsystem (7) or (8) can be analyzed only in the regions where this subsystem is active. The behavior of this subsystem in other parts of the state space does not influence the original PWS system. Consequently, our stability analysis of the continuous PWS system (3) can be done under such justification because the sliding motion is ruled out.

In this context, it is useful to recall some definitions related to the classification of equilibria that a PWS system may possess [38]. On the one hand, a point $\mathbf{X}^* \in \mathbb{R}^3_+$ satisfying either

$$\mathbf{\Phi}_1(\mathbf{X}^*) = \mathbf{0} \quad \text{and} \quad \mathbf{X}^* \in \mathbb{M}_a$$

or

$$\mathbf{\Phi}_2(\mathbf{X}^*) = \mathbf{0} \quad \text{and} \quad \mathbf{X}^* \in \mathbb{M}_s$$

is referred to as a *regular equilibrium* of the PWS system (3). On the other hand, a point $\mathbf{X}^* \in \mathbb{R}^3_+$ satisfying either

$$\mathbf{\Phi}_1(\mathbf{X}^*) = \mathbf{0} \quad \text{and} \quad \mathbf{X}^* \in \mathbb{M}_s$$

or

$$\mathbf{\Phi}_2(\mathbf{X}^*) = \mathbf{0} \quad \text{and} \quad \mathbf{X}^* \in \mathbb{M}_a$$

is called a *virtual equilibrium* of the PWS system (3).

Let us also introduce for future use the following positive quantities:

$$\mathcal{N}_M := \frac{\gamma r \rho \nu}{\mu(\delta+\eta)} = \frac{r\rho}{\mu}\cdot\frac{\gamma\nu}{\delta+\eta}, \qquad \mathcal{N}_F := \frac{(1-r)\rho\nu}{\delta(\delta+\eta+\nu)} = \frac{(1-r)\rho}{\delta}\cdot\frac{\nu}{\delta+\eta+\nu}. \tag{9}$$

These positive constants represent the *basic offspring numbers* [41] related to the male and female psyllids. It is worthwhile to recall that the basic offspring number $\mathcal{N}_M$ (resp. $\mathcal{N}_F$) expresses a mean number of male (resp. female) descendants produced by one male (resp. female) individual during his (resp. her) her lifespan. For males, $\mathcal{N}_M$ depends not only on the usual ratio $r\rho/\mu$ expressing an average number of eggs that later become males but also on the mating efficiency γ of males and the relative availability for mating $\nu/(\delta+\nu)$ of the female psyllids. Similarly, for females, $\mathcal{N}_F$ depends not only on the usual ratio $(1-r)\rho/\delta$ expressing an average number of eggs that later become females but also on the mating frequency of female psyllids $\nu/(\delta+\eta+\nu)$. Notably, the parameters ν, η related to the interchange between the compartments A and U are explicitly included in $\mathcal{N}_M$ and $\mathcal{N}_F$ meaning that the

overall population size of adult insects strongly depends on the females' readiness for mating.

Now we proceed to identify the possible equilibria of smooth ODE systems (7) and (8).

3.1. Case 1: abundance of male psyllids

When $\gamma M > A$, the PWS system (1) becomes (7) with $\mathbf{\Phi}_1$ given by (4). As we are interested only in biologically meaningful behavior of this system, its equilibria are nonnegative solutions of the following algebraic system

$$\begin{cases} 0 = r\rho U e^{-\sigma(M+A+U)} - \mu M, & \text{(10a)} \\ 0 = (1-r)\rho U e^{-\sigma(M+A+U)} - \nu A + \eta U - \delta A, & \text{(10b)} \\ 0 = \nu A - \eta U - \delta U. & \text{(10c)} \end{cases}$$

It is immediate to deduce that $\mathbf{E}_0 = (0,0,0)$ is solution of (10). Then, we solve this system with M and A as unknowns and obtain

$$M = \frac{r\delta(\delta+\eta+\nu)}{(1-r)\mu\nu}U, \qquad A = \frac{(\delta+\eta)}{\nu}U. \tag{11}$$

Replacing these solutions in (10a), we obtain

$$r\rho U e^{-\sigma(M+A+U)} = \frac{\delta r(\delta+\eta+\nu)}{\nu(1-r)}U \quad \Rightarrow \quad e^{-\sigma(M+A+U)} = \frac{\delta(\delta+\eta+\nu)}{(1-r)\rho\nu} = \frac{1}{\mathcal{N}_F}$$

according to the second relationship in (9). Thus, we deduce

$$M + A + U = \frac{1}{\sigma}\ln\mathcal{N}_F > 0, \tag{12}$$

meaning that a positive solution $\mathbf{E}_1^* := \left(M_1^*, A_1^*, U_1^*\right)$ of (10) exists if and only if $\mathcal{N}_F > 1$. Further, by plugging the relationships (11) into (12) we obtain

$$\frac{1}{\sigma}\ln\mathcal{N}_F = \left(\frac{r\delta(\delta+\eta+\nu)}{(1-r)\mu\nu} + \frac{(\delta+\eta)}{\nu} + 1\right)U = \frac{(\delta+\eta+\nu)\vartheta}{(1-r)\mu\nu}U, \tag{13}$$

where

$$\vartheta := (1-r)\mu + r\delta \tag{14}$$

denotes the so-called *standardized mortality* of adult psyllids that, in effect, is the weighted mean mortality of both sex groups with the weights defined by their opposite-sex ratios. Finally, solving Eq. (13) for U and using it in (11) we arrive to a strictly positive solution $\mathbf{E}_1^* := \left(M_1^*, A_1^*, U_1^*\right)$ of (10):

$$\begin{cases} M_1^* = r\dfrac{\delta}{\vartheta}\dfrac{1}{\sigma}\ln\mathcal{N}_F, & \text{(15a)} \\ A_1^* = (1-r)\dfrac{\mu}{\vartheta}\dfrac{\delta+\eta}{(\delta+\eta+\nu)}\dfrac{1}{\sigma}\ln\mathcal{N}_F, & \text{(15b)} \\ U_1^* = (1-r)\dfrac{\mu}{\vartheta}\dfrac{\nu}{(\delta+\eta+\nu)}\dfrac{1}{\sigma}\ln\mathcal{N}_F. & \text{(15c)} \end{cases}$$

Note also that the total number of insects at equilibrium $\mathbf{E}_1^*$ verifies (12), and its coordinates explicitly include the standardized mortality ratios ($r\delta/\vartheta$ and $(1-r)\mu/\vartheta$) related to opposite sex.

Thus, we conclude that the smooth system (7) has two possible equilibria: the trivial equilibrium $\mathbf{E}_0 = (0,0,0)$ that exists for any positive value of $\mathcal{N}_F$ (defined by (9)), and the strictly positive one $\mathbf{E}_1^* = \left(M_1^*, A_1^*, U_1^*\right)$ defined by (15) that exists if and only if $\mathcal{N}_F > 1$. The following result establishes the stability properties of $\mathbf{E}_0$ and $\mathbf{E}_1^*$.

Proposition 2. *Consider the ODE system (7) with $\mathbf{\Phi}_1(\mathbf{X})$ defined by (4). Then the following statements are valid:*

(i) *If $\mathcal{N}_F < 1$, the trivial equilibrium $\mathbf{E}_0$ is locally asymptotically stable (LAS, in the sequel).*

(ii) *If $\mathcal{N}_F > 1$, a strictly positive equilibrium $\mathbf{E}_1^*$ defined by (15) is LAS, and $\mathbf{E}_0$ is unstable; however, there always exists a trajectory converging to $\mathbf{E}_0$ meaning that $\mathbf{E}_0$ is not a repeller.*

Proof. See Appendix A . ■

3.2. Case 2: scarcity of male psyllids

When $\gamma M < A$, the PWS system (1) becomes (8) with $\mathbf{\Phi}_2$ given by (5), and its equilibria are nonnegative solutions of the following algebraic system

$$\begin{cases} 0 = r\rho U e^{-\sigma(M+A+U)} - \mu M, & \text{(16a)} \\ 0 = (1-r)\rho U e^{-\sigma(M+A+U)} - \gamma\nu M + \eta U - \delta A, & \text{(16b)} \\ 0 = \gamma\nu M - \eta U - \delta U. & \text{(16c)} \end{cases}$$

It is immediate to deduce that $\mathbf{E}_0 = (0,0,0)$ is solution of (16). We also set

$$\theta_M := \frac{(1-r)\mu(\delta+\eta)}{\gamma r\delta\nu}. \tag{17}$$

Then, we solve the nonlinear system (16) with M and A as unknowns and obtain

$$M = \frac{(\delta+\eta)}{\gamma\nu}U, \qquad A = \left(\frac{\mu(1-r)(\delta+\eta)}{\gamma\delta\nu r} - 1\right)U = \left(\theta_M - 1\right)U. \tag{18}$$

Thus, $A > 0$ whenever $\theta_M > 1$. It is interesting to notice that

$$\theta_M = \frac{1}{\mathcal{N}_M}\frac{(1-r)\rho}{\delta},$$

such that having $\mathcal{N}_M > 1$ (cf. the first relationship in (9)), we need

$$\frac{(1-r)\rho}{\delta} > \mathcal{N}_M, \tag{19}$$

in order to assure that $\theta_M > 1$. In fact, (19) means that the average number of eggs that further become females has to be larger than the mean number of male descendants produced by one male individual all along his lifespan. In other words, condition $\theta_M > 1$ can be replaced by (19).

Direct substitution of (18) into (16a) renders

$$r\rho U e^{-\sigma(A+M+U)} = \frac{\mu(\delta+\eta)}{\gamma\nu}U \quad \Rightarrow \quad e^{-\sigma(A+M+U)} = \frac{\mu(\delta+\eta)}{\gamma r\rho\nu} = \frac{1}{\mathcal{N}_M}$$

leading to

$$A + M + U = \frac{1}{\sigma}\ln\mathcal{N}_M > 0, \tag{20}$$

and meaning that a positive solution $\mathbf{E}_2^* = \left(M_2^*, A_2^*, U_2^*\right)$ of (16) exists if and only if $\mathcal{N}_M > 1$ and $\theta_M > 1$, where $\mathcal{N}_M$ and θ_M are given by (9) and (17), respectively. Further, by plugging the relationships (18) into (20) we obtain

$$\frac{1}{\sigma}\ln\mathcal{N}_M = M + A + U = \left(\frac{\eta+\delta}{\nu\gamma} + \theta_M - 1 + 1\right)U = \frac{\gamma\nu\theta_M + \eta + \delta}{\gamma\nu}U. \tag{21}$$

Finally, solving Eq. (21) for U and using it in (18) we arrive to a strictly positive solution $\mathbf{E}_2^* := \left(M_2^*, A_2^*, U_2^*\right)$ of (16):

$$\begin{cases} M_2^* = \dfrac{\delta+\eta}{\gamma\nu\theta_M + \eta + \delta}\dfrac{1}{\sigma}\ln\mathcal{N}_M, & \text{(22a)} \\ A_2^* = \dfrac{\gamma\nu\left(\theta_M - 1\right)}{\gamma\nu\theta_M + \eta + \delta}\dfrac{1}{\sigma}\ln\mathcal{N}_M, & \text{(22b)} \\ U_2^* = \dfrac{\gamma\nu}{\gamma\nu\theta_M + \eta + \delta}\dfrac{1}{\sigma}\ln\mathcal{N}_M. & \text{(22c)} \end{cases}$$

Remark 1. One can also obtain the expressions for coordinates of $\mathbf{E}_2^*$ in terms of the standardized mortality ϑ defined by (14). Notably, the denominator of all expressions included in (22) verifies

$$\gamma\nu\theta_M + \eta + \delta = \gamma\nu\frac{(1-r)\mu(\delta+\eta)}{\gamma r\delta\nu} + (\delta+\eta)$$
$$= (\delta+\eta)\left(\frac{(1-r)\mu}{r\delta} + 1\right) = (\delta+\eta)\frac{\vartheta}{r\delta}.$$

Furthermore,

$$\gamma\nu(\theta_M - 1) = \frac{(1-r)\mu(\delta+\eta)}{r\delta} - \gamma\nu = \frac{\mu}{r}(\delta+\eta)\left(\frac{1-r}{\delta} - \frac{\gamma r\nu}{\mu(\delta+\eta)}\right)$$
$$= \frac{\mu}{r\rho}(\delta+\eta)\left(\frac{(1-r)\rho}{\delta} - \mathcal{N}_M\right).$$

Using the above relationships in combination with (22), we can obtain an alternative form of (22):

$$\begin{cases} M_2^* = r\dfrac{\delta}{\vartheta}\dfrac{1}{\sigma}\ln\mathcal{N}_M, & \text{(23a)} \\ A_2^* = \dfrac{\mu}{\vartheta}\dfrac{\delta}{\rho}\left(\dfrac{(1-r)\rho}{\delta} - \mathcal{N}_M\right)\dfrac{1}{\sigma}\ln\mathcal{N}_M, & \text{(23b)} \\ U_2^* = \dfrac{\mu}{\vartheta}\dfrac{\delta}{\rho}\mathcal{N}_M\dfrac{1}{\sigma}\ln\mathcal{N}_M. & \text{(23c)} \end{cases}$$

This alternative form of $\mathbf{E}_2^*$ makes visible the necessity of the condition (19) for existence of $\mathbf{E}_2^*$ along with $\mathcal{N}_M > 1$.

Note also that for both forms of $\mathbf{E}_2^*$ ((22) and (23)), the total number of insects at equilibrium $\mathbf{E}_2^*$ verifies (20).

Thus, we conclude that the smooth system (8) has two possible equilibria: the trivial equilibrium $\mathbf{E}_0 = (0,0,0)$ that exists for any positive value of $\mathcal{N}_M$ (defined by (9)), and the strictly positive one $\mathbf{E}_2^* = (M_2^*, A_2^*, U_2^*)$ defined by (22) or (23) that exists if and only if $\mathcal{N}_M > 1$ and $\theta_M > 1$, that is, if the condition (19) holds. The following result establishes the stability properties of $\mathbf{E}_0$ and $\mathbf{E}_2^*$.

Proposition 3. *Consider the ODE system (8) with $\mathbf{\Phi}_2(\mathbf{X})$ defined by (5). Then the following statements are valid:*

(i) *If $\mathcal{N}_M < 1$, the trivial equilibrium $\mathbf{E}_0$ is LAS.*

(ii) *If $\mathcal{N}_M > 1$, a strictly positive equilibrium $\mathbf{E}_2^*$ defined by either (22) or (23) is LAS, and $\mathbf{E}_0$ is unstable; however, there always exists a trajectory converging to $\mathbf{E}_0$ meaning that $\mathbf{E}_0$ is not a repeller.*

Proof. See Appendix A . ■

3.3. Stability analysis of the PWS system (1).

First, we note that $\mathbf{E}_0 \in \mathcal{P}_s$. Let us now determine the position of $\mathbf{E}_1^*$ and $\mathbf{E}_2^*$ in $\mathbb{R}^3_+$ with respect to the switching plane $\mathcal{P}_s$. Clearly, $\mathbf{E}_1^* \in \mathcal{P}_s$ if and only if $\gamma M_1^* = A_1^*$, that is,

$$\gamma r\frac{\delta}{\vartheta}\frac{1}{\sigma}\ln\mathcal{N}_F = (1-r)\frac{\mu}{\vartheta}\frac{\delta+\eta}{(\delta+\eta+\nu)}\frac{1}{\sigma}\ln\mathcal{N}_F \quad \text{or} \quad \gamma r\delta = (1-r)\mu\frac{\delta+\eta}{(\delta+\eta+\nu)}.$$

By multiplying both sides of the last relationship by $\dfrac{\rho\nu}{\mu\delta(\delta+\eta)} > 0$ we arrive to

$$\frac{\gamma r\rho\nu}{\mu(\delta+\eta)} = \frac{(1-r)\rho\nu}{\delta(\delta+\eta+\nu)} \quad \Leftrightarrow \quad \mathcal{N}_M = \mathcal{N}_F.$$

Thus, $\mathbf{E}_1^* \in \mathcal{P}_s$ if and only if $\mathcal{N}_M = \mathcal{N}_F > 1$. Furthermore, it is easy to deduce that

$$\mathbf{E}_1^* \in \mathbb{M}_a \quad \Leftrightarrow \quad \mathcal{N}_M > \mathcal{N}_F > 1 \quad \text{and} \quad \mathbf{E}_1^* \in \mathbb{M}_s \quad \Leftrightarrow \quad \mathcal{N}_M < \mathcal{N}_F,\ \mathcal{N}_F > 1.$$

The above expressions imply that $\mathbf{E}_1^*$ is a *regular equilibrium* of the original PWS system (1) when $\mathcal{N}_M > \mathcal{N}_F > 1$, and $\mathbf{E}_1^*$ is a *virtual equilibrium* of (1) when $\mathcal{N}_M < \mathcal{N}_F$ and $\mathcal{N}_F > 1$.

In its turn, $\mathbf{E}_2^* \in \mathcal{P}_s$ if and only if $\gamma M_2^* = A_2^*$, that is,

$$\frac{\gamma(\delta+\eta)}{\gamma\nu\theta_M + \eta + \delta}\frac{1}{\sigma}\ln\mathcal{N}_M = \frac{\nu\gamma(\theta_M - 1)}{\gamma\nu\theta_M + \eta + \delta}\frac{1}{\sigma}\ln\mathcal{N}_M \quad \text{or}$$
$$\delta + \eta + \nu = \frac{\nu(1-r)\mu(\delta+\eta)}{\gamma r\delta\nu}.$$

By multiplying both sides of the last relationship by $\dfrac{\gamma r\rho\nu}{\mu(\delta+\eta)(\delta+\eta+\nu)} > 0$ we arrive to

$$\frac{\gamma r\rho\nu}{\mu(\delta+\eta)} = \frac{(1-r)\rho\nu}{\delta(\delta+\eta+\nu)} \quad \Leftrightarrow \quad \mathcal{N}_M = \mathcal{N}_F.$$

Thus, $\mathbf{E}_2^* \in \mathcal{P}_s$ if and only if $\mathcal{N}_M = \mathcal{N}_F > 1$. Furthermore, it is easy to deduce that

$$\mathbf{E}_2^* \in \mathbb{M}_s \quad \Leftrightarrow \quad \mathcal{N}_F > \mathcal{N}_M > 1 \quad \text{and} \quad \mathbf{E}_2^* \in \mathbb{M}_a \quad \Leftrightarrow \quad \mathcal{N}_M > \mathcal{N}_F,\ \mathcal{N}_M > 1.$$

The above expressions imply that $\mathbf{E}_2^*$ is a *regular equilibrium* of the original PWS system (1) when $\mathcal{N}_F > \mathcal{N}_M > 1$, and $\mathbf{E}_2^*$ is a *virtual equilibrium* of (1) when $\mathcal{N}_M > \mathcal{N}_F$ and $\mathcal{N}_M > 1$. Fig. 3 schematically displays the regular and virtual equilibria the PWS system (3)–(5) may possess according to the values of the basic offspring numbers $\mathcal{N}_F$ and $\mathcal{N}_M$.

From the foregoing rationale, we can also conclude that $\mathcal{N}_M = \mathcal{N}_F > 1$ implies that $\mathbf{E}_1^* = \mathbf{E}_2^* \in \mathcal{P}_s$ meaning that both positive equilibria collide and coalesce on the switching plane $\mathcal{P}_s$. The latter can be checked by comparing the components of $\mathbf{E}_1^*$ and $\mathbf{E}_2^*$ using their forms given by (15) and (23) when $\mathcal{N}_M = \mathcal{N}_F > 1$.

It is worth recalling that the values of $\mathcal{N}_M$ and $\mathcal{N}_F$ are defined by the model's parameters (cf. (9)), they remain unchanged, and the behavior of the PWS system (3) is determined by the relationship between $\mathcal{N}_M$ and $\mathcal{N}_F$ as indicated in Fig. 3. Among different options shown in Fig. 3, the realistic one is the case of viable populations, that is when $\mathcal{N}_M > 1$ and $\mathcal{N}_F > 1$ (meaning that each male/female individual produced more than one male/female individual during his/her lifespan). Let us also recall that the PWS system is autonomous, continuous, and exhibits only constrained state-dependent switching. Therefore, according to [40], the behavior of the PWS system (3) is determined by the behavior of its subsystems (7) and (8) in the regions where these subsystems are active. This leads us to the following summary:

- If $\mathcal{N}_M > \mathcal{N}_F > 1$ and $(M_0, A_0, U_0) \in \mathbb{M}_a$ (meaning that $\gamma M_0 \geq A_0$), the evolution of the PWS system (3) will be the same as of its ODE subsystem (7) with mating function $\min\left\{\dfrac{\gamma M}{A}, 1\right\} = 1$, implying convergence to the regular equilibrium $\mathbf{E}_1^*$ starting from $t \geq 0$ (no crossing through the switching plane $\mathcal{P}_s$).
- If $\mathcal{N}_F > \mathcal{N}_M > 1$ and $(M_0, A_0, U_0) \in \mathbb{M}_s$ (meaning that $\gamma M_0 < A_0$), the evolution of the PWS system (3) will be the same as of its ODE subsystem (8) with mating function $\min\left\{\dfrac{\gamma M}{A}, 1\right\} = \dfrac{\gamma M}{A}$, implying convergence to the regular equilibrium $\mathbf{E}_2^*$ starting from $t \geq 0$ (no crossing through the switching plane $\mathcal{P}_s$).
- If $\mathcal{N}_M > \mathcal{N}_F > 1$ but $(M_0, A_0, U_0) \in \mathbb{M}_s$ (meaning that $\gamma M_0 < A_0$), the evolution of the PWS system will be the same as of its ODE subsystem (8) with mating function $\min\left\{\dfrac{\gamma M}{A}, 1\right\} = \dfrac{\gamma M}{A}$ up to some finite time $t_s > 0$, satisfying the relationship $\gamma M(t_s) = A(t_s)$, at which the crossing through the switching plane $\mathcal{P}_s$ will take place. Further on, for $t > t_s$, the evolution of the PWS system will be the same as of its ODE subsystem (7) with mating function $\min\left\{\dfrac{\gamma M}{A}, 1\right\} = 1$, implying ultimate convergence to the regular equilibrium $\mathbf{E}_1^*$.
- If $\mathcal{N}_F > \mathcal{N}_M > 1$ but $(M_0, A_0, U_0) \in \mathbb{M}_a$ (meaning that $\gamma M_0 \geq A_0$), the evolution of the PWS system will be the same as of its ODE subsystem (7) with mating function $\min\left\{\dfrac{\gamma M}{A}, 1\right\} = 1$ up to some finite time $t_s > 0$, satisfying the relationship $\gamma M(t_s) = A(t_s)$, at which the crossing through the switching plane $\mathcal{P}_s$ will take place. Further on, for $t > t_s$, the evolution of the PWS system will be the same as of its ODE subsystem (8) with mating function $\min\left\{\dfrac{\gamma M}{A}, 1\right\} = \dfrac{\gamma M}{A}$, implying ultimate convergence to the regular equilibrium $\mathbf{E}_2^*$.

The last two situations exhibiting the crossing through the switching plane $\mathcal{P}_s$ are illustrated in Fig. 4, where the solutions of the PWS system (3) are plotted by solid curves and the solutions of the ODE systems (7)

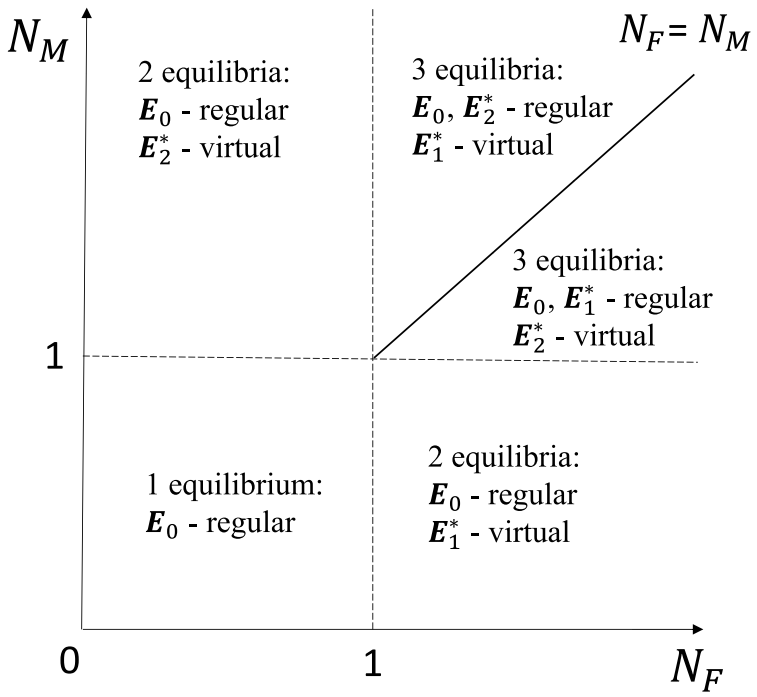

Fig. 3. Regular and virtual equilibria of the PWS system (3)–(5) according to the values of $\mathcal{N}_F$ and $\mathcal{N}_M$.

and (8) are drawn by dotted lines on the left and right upper charts, respectively.

Looking at the left-hand upper chart in Fig. 4, we can observe that the components of the PWS system (3) (solid curves) behave unlike those of the ODE system (7) (dotted curves) because, starting from the initial point $(M_0, A_0, U_0) \in \mathbb{M}_s$ the relationship $\gamma M(t) < A(t)$ remains in force for small values of $t \geq 0$ meaning that the PWS system follows the dynamics of the ODE subsystem (8).

However, the trajectories $\big(M(t), A(t), U(t)\big)$ of the PWS system (3) eventually reach the switching plane $\mathcal{P}_s$ and cross it at some finite time $t = t_s > 0$ because the parameters of the PWS system (3) satisfy the relationship $\mathcal{N}_M > \mathcal{N}_F > 1$. Thus, after crossing the switching plane $\mathcal{P}_s$, the components of the PWS system (3) (solid curves), as well as those of the ODE system (7) (dotted curves) converge to the same equilibrium $\mathbf{E}_1^*$. The left-hand lower chart in Fig. 4 illustrates the behavior of the mating function that is increasing and reaches the unity value from below at some $t = t_s$ and then remains equal to 1.

Similarly, the right-hand upper chart in Fig. 4 illustrates that the components of the PWS system (3) (solid curves) behave unlike those of the ODE subsystem (8) (dotted curves) when the relationship $\gamma M(t) > A(t)$ remains in force for small values of $t \geq 0$ meaning that the PWS system follows the dynamics of the ODE subsystem (7). As the parameters of the PWS system fulfill the relation $\mathcal{N}_F > N_M > 1$, the mating function will eventually drop below the unity value at some $t = t_s > 0$ (see the right-hand lower chart in Fig. 4), and the trajectories of the PWS system (3) (solid curves) will cross the switching plane $\mathcal{P}_s$. Thus, the trajectories of the PWS system will start following the dynamics of the ODE subsystem (8), and the latter implies convergence towards the equilibrium $\mathbf{E}_2^*$.

Even though the solid and dotted curves at each upper chart exhibit different behavior for relatively small $t \geq 0$, their further evolution is the same. This outcome stems from the corresponding forms of the mating functions presented on the lower charts in Fig. 4 where $t = t_s$ marks the switching time. It is worthwhile to note that both cases in Fig. 4 are obtained for the same parameters values given in Table 1, except for γ: when $\gamma = 1.2$, we have $\mathcal{N}_M > \mathcal{N}_F > 1$ (the left-hand column of Fig. 4), while with $\gamma = 1$, we have $\mathcal{N}_F > \mathcal{N}_M > 1$ (the right-hand column of Fig. 4).

Other situations plotted in Fig. 3 are less interesting from the practical standpoint. Nonetheless, let us briefly comment on them from the mathematical viewpoint.

First, when $\mathcal{N}_M < 1$ and $N_F < 1$, the ACP population is plainly unviable and cannot persist. Moreover, neither $\mathbf{E}_1^*$ nor $\mathbf{E}_2^*$ exist (their coordinates become negative, cf. (15), (23)). Therefore, $\mathbf{E}_0$ is a unique asymptotically stable equilibrium of both subsystems (7) and (8) as proved by Propositions 2 and 3. The latter implies that no matter which of the two subsystems is in action, the evolution of the continuous PWS system (3) leads to population extinction. In fact, one can deduce that two outcomes are possible, namely:

- $\mathbf{E}_0$ will be approached from the side of $\mathbb{M}_a$ if the population of females declines faster the that of males ($\mathcal{N}_F < \mathcal{N}_M < 1$) meaning that subsystem (7) will ultimately come into action.
- $\mathbf{E}_0$ will be approached from the side of $\mathbb{M}_s$ if the population of males declines faster the that of females ($\mathcal{N}_M < \mathcal{N}_F < 1$) meaning that subsystem (8) will ultimately come into action.

Second, when $\mathcal{N}_M < 1 < \mathcal{N}_F$, the steady state E_1^* of subsystem (7) still exists, while the steady state E_2^* of subsystem (8) does not. Even if the initial condition satisfies the relationship $\gamma M_0 > A_0$ meaning that subsystem (7) will act for smaller values of $t \geq 0$, the population of males, $M(t)$, will steadily decline because $\mathcal{N}_M < 1$ implies that each male insect produces less than one male insect during his lifespan. Therefore, the mating function will eventually drop below the unity value, and the subsystem (8) will come into action. As proved by Proposition 3, $\mathbf{E}_0$ is LAS when $\mathcal{N}_M < 1$, and the ACP population will go to extinction. This implies that $\mathbf{E}_0$ is a regular equilibrium of the PWS system (3) while E_1^* is a virtual one.

Similarly, when $\mathcal{N}_F < 1 < \mathcal{N}_M$, the steady state E_2^* of subsystem (8) still exists, while the steady state E_1^* of subsystem (7) does not. Even if the initial condition satisfies the relationship $\gamma M_0 < A_0$ meaning that subsystem (8) will act for smaller values of $t \geq 0$, the population of all females, $F(t) = A(t) + U(t)$, will steadily decline because $\mathcal{N}_F < 1$ implies that each female insect produces less than one female insect during

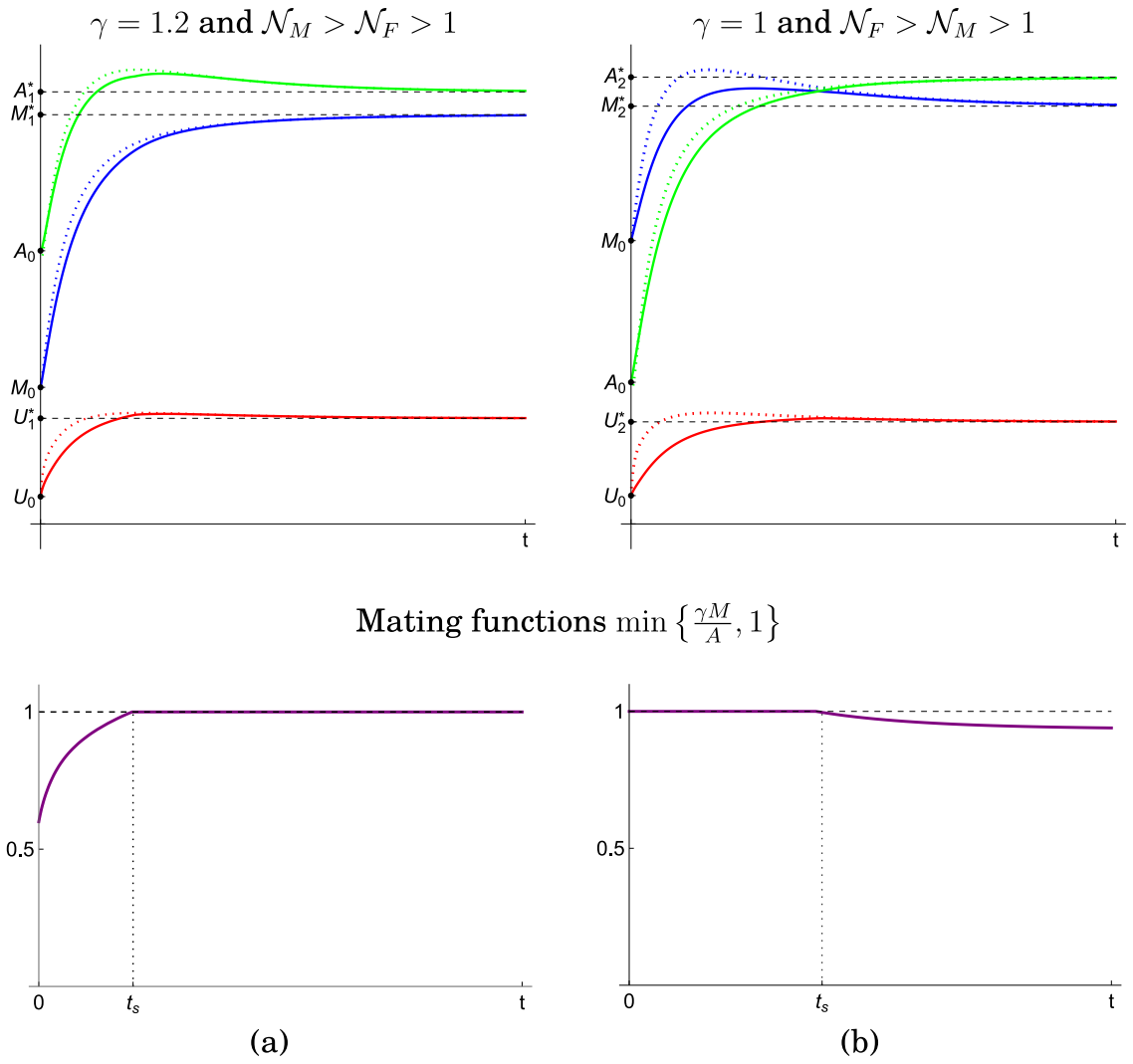

Fig. 4. Behavior of the PWS system (3) and its two subsystems (7) and (8): (a) *upper row*: trajectories of the PWS system (3) (solid curves) and trajectories of the ODE system (7) (dotted curves) engendered by $(M_0, A_0, U_0) = (500, 1000, 100) \in \mathbb{M}_s$; *lower row*: mating function of the PWS system (3); (b) *upper row*: trajectories of the PWS system (3) (solid curves) and trajectories of the ODE system (8) (dotted curves) engendered by $(M_0, A_0, U_0) = (1000, 500, 100) \in \mathbb{M}_a$; *lower row*: mating function of the PWS system (3).

her lifespan. Therefore, the mating function will eventually reach the unity value, and the subsystem (7) will come into action. As proved by Proposition 2, $\mathbf{E}_0$ is LAS when $\mathcal{N}_F < 1$, and the ACP population will go to extinction. This implies that $\mathbf{E}_0$ is a regular equilibrium of the PWS system (3) while E_2^* is a virtual one.

To complete this section, we would like to underline that the primary objective of this study is to demonstrate the possibility and efficacy of pheromone-based mating disruption and male-targeted trapping in reducing *D. citri* populations when these are already near a LAS equilibrium, and the next sections are devoted to this purpose.

We are aware that issues related to global stability, the possible appearance of other attractors, and bifurcation analysis are mathematically important and biologically relevant, and must also be studied. However, they are beyond the scope of the present work. Each of these analyses introduces significant technical and computational complexity that would detract from the main message: namely, that control strategies based on male disruption can be effective in realistic ecological conditions. These topics are thus reserved for future studies, where they can be treated with the depth and rigor they require without overextending the current manuscript.

4. Pest control by pheromone traps

Female psyllids available for mating (class A) emit sex pheromones that attract male insects over a long distance [42]. Using sex pheromone control and mating disruption for managing pests like *D. citri*, instead of traditional insecticide spraying, offers several ecological, economic, and agricultural benefits, namely:

- Sex pheromones are species-specific, volatile, and biodegradable. Compared to broad-spectrum pesticides and insecticides, which can contaminate soil, water, air, and fruits, sex pheromones have a lower environmental impact.
- Pheromone-based intervention does not involve toxic chemicals that could pose risks to farmers, consumers, or wildlife. However, Insecticide exposure can lead to acute or chronic health issues.
- Continuous use of chemical substances may lead to resistance in pest populations, while pheromone based mating disruption targets the insects communication system, thus reducing the likelihood of resistance development.
- Compared to repeated insecticide spraying, which only kills present pests but can also lead to their immediate resurgence,

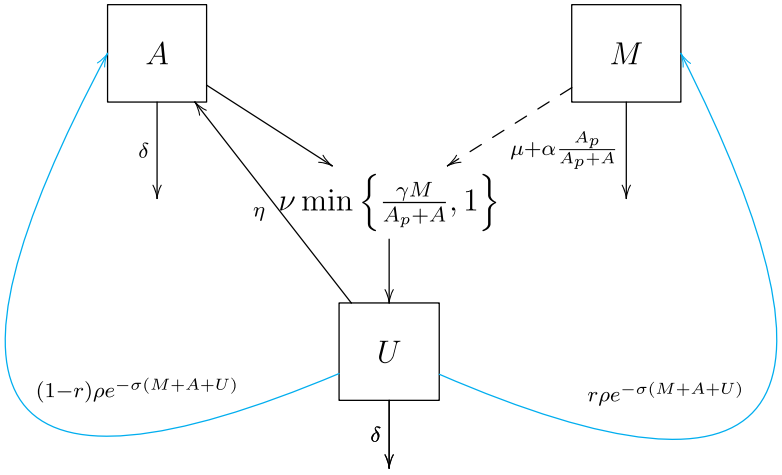

Fig. 5. Flow diagram of the ACP population dynamics with pheromone traps (24).

mating disruption interferes with the insects ability to reproduce and gradually lowers the population density over time, making a more sustainable, long-term impact on reducing the pest population.

Therefore, sex pheromone traps may offer an alternative to traditional chemical control measures and can be considered an eco-friendly component of integrated pest control. First, pheromone traps can be used for monitoring pest insects to determine whether additional control measures are needed [43]. Second, pheromone traps can be set up as a lure to perform control of pest populations [44]. In this case, sticky pheromone traps emitting large quantities of sex pheromones may serve one of the following two purposes or both of them:

1. Attraction and mass trapping of male insects, followed by their direct removal (male killing).
2. Mating disruption for decreasing the fecundity of females (offspring reduction).

The ACP population dynamics model (1) proposed in Section 2 can be adapted to include the two control actions mentioned above, and the present section encompasses the analysis of the long-term performance of pheromone traps plugged in natural populations of adult psyllids. Let $A_p > 0$ express the "strength of lure". Knowing the average amount of sex pheromones emitted by one female psyllid [45], the control parameter A_p can be expressed in terms of the number of "false" female psyllids available for mating. Then, the total number of male-seeking females (both natural and false) is expressed by $(A_p + A)$ [21,33]. Furthermore, a female-seeking male has the probability $\frac{A}{A_p+A}$ of being attracted to a wild (natural) female and the probability $\frac{A_p}{A_p+A}$ of being attracted to the pheromone traps. Let $\alpha \in [0,1]$ denote the capture or killing rate of males attracted to a pheromone trap. Then, by setting $\alpha = 1$, it is modeled that all males approaching or entering the trap are killed, while $\alpha = 0$ models that none of them will be killed when approaching or entering the trap. Notably, by setting $\alpha = 0$ and $A_p = 0$, the original model (1) can be immediately recovered.

Using two additional parameters (A_p and α) defined above, we can now formulate the modified version of the model (1) that accounts for mating disruption and male-killing effect induced by the pheromone traps:

$$\begin{cases} \dfrac{dM}{dt} = r\rho U e^{-\sigma(M+A+U)} - \alpha\dfrac{A_p}{A_p+A}M - \mu M, & \text{(24a)} \\ \dfrac{dA}{dt} = (1-r)\rho U e^{-\sigma(M+A+U)} - \nu \min\left\{\dfrac{\gamma M}{A_p+A}, 1\right\} A + \eta U - \delta A, & \text{(24b)} \\ \dfrac{dU}{dt} = \nu \min\left\{\dfrac{\gamma M}{A_p+A}, 1\right\} A - \eta U - \delta U. & \text{(24c)} \end{cases}$$

The initial conditions for this model are the same as (2), and Fig. 5 provides the flow diagram of the model (24).

Similarly to the original dynamical system (1), the model (24) is an autonomous continuous PWS system that features two control parameters $\alpha \in [0,1]$ and $A_p \geq 0$, one of which directly affects its switching plane

$$\widetilde{\mathcal{P}}_s(A_p) := \left\{(M,A,U) \in \mathbb{R}^3_+ : \ \gamma M = A + A_p\right\}$$

that now depends also on $A_p > 0$, and the threshold of the mating function $\min\left\{\dfrac{\gamma M}{A_p+A}, 1\right\}$ turns into $\gamma M = A + A_p$. Similar to the uncontrolled PWS system (1), system (24) exhibits only a constrained state-dependent switching when both parameters $\alpha \in [0,1]$ and A_p remain constant. Therefore, the trajectories of (24) may only cross the switching plane $\widetilde{\mathcal{P}}_s(A_p)$ transversely, and no sliding motion constrained to $\widetilde{\mathcal{P}}_s(A_p)$ can take place [38,39]. It is worth mentioning that the existence and uniqueness of a nonnegative uniformly ultimately bounded solution to the system can be justified using the same rationale as employed in Section 2. The geometric role of the parameter $A_p > 0$ is illustrated in Fig. 6: for larger values of $A_p > 0$, the male-scarcity region becomes more extensive, and the switching plane $\widetilde{\mathcal{P}}_s(A_p)$ moves farther away from the origin.

Existence and uniqueness of a piecewise smooth solution to the system (24) for any nonnegative initial conditions (2), as well as the nonnegativity and boundedness of the system's trajectories in $\mathbb{R}^3_+$ can be proved using the arguments presented in the proof of Proposition 1.

It is worthwhile to recall that the qualitative analysis of continuous PWS systems exhibiting only a constrained state-dependent switching can be facilitated by splitting it into two subsystems and studying the fundamental properties of its subsystems only in the regions where each subsystem is active [40]. Following the approach in Section 3, we split the PWS system (24) into two smooth systems, each featuring two parameters of control, α and A_p.

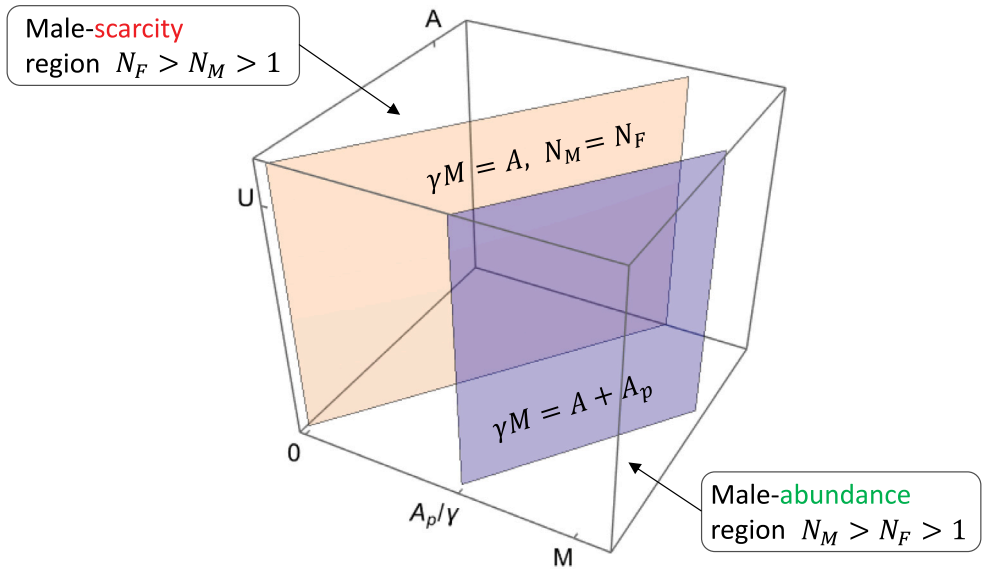

Fig. 6. Changes in the male-scarcity and male-abundance regions induced by $A_p > 0$.

For each smooth ODE subsystem, we propose two operational control modes referred to as open-loop (or feed-forward) and closed-loop (or feedback) control approaches, both requiring to estimate the ACP population size before the treatment starts. The open-loop control operates based on a predefined sequence of actions. Thus, in the context of pheromone trapping, it avoids the real-time monitoring of the psyllid population sizes and requires to define, for any fixed $\alpha \in [0,1]$, a constant value of $A_p > 0$ to be used for the whole treatment taking into account only the size of the initial ACP population. In contrast, the closed-loop control approach is more adaptive since its actions can respond to changes in the system behavior. Therefore, in the context of mating disruption, it involves periodic assessments of the ACP population size, allowing for adjustments of A_p (also for any fixed $\alpha \in [0,1]$) based on real-time estimation data and proportionally to the current ACP population size.

4.1. Open-loop control approach

Let us assume that the male-killing rate $\alpha \in [0,1]$ and the emission rate of sex pheromones $A_p > 0$ will remain constant during the entire time of the control intervention. In the male abundance region $\mathbb{M}_a$, where it holds $\gamma M > A + A_p$, the dynamical system (24) takes the following form:

$$\begin{cases} \dfrac{dM}{dt} = r\rho U e^{-\sigma(M+A+U)} - \alpha \dfrac{A_p}{A_p + A} M - \mu M, & \text{(25a)} \\ \dfrac{dA}{dt} = (1-r)\rho U e^{-\sigma(M+A+U)} - \nu A + \eta U - \delta A, & \text{(25b)} \\ \dfrac{dU}{dt} = \nu A - \eta U - \delta U, & \text{(25c)} \end{cases}$$

and in the male-scarcity region $\mathbb{M}_s$, where it holds $\gamma M < A + A_p$, the dynamical system (24) becomes:

$$\begin{cases} \dfrac{dM}{dt} = r\rho U e^{-\sigma(M+A+U)} - \alpha \dfrac{A_p}{A_p + A} M - \mu M, & \text{(26a)} \\ \dfrac{dA}{dt} = (1-r)\rho U e^{-\sigma(M+A+U)} - \nu \dfrac{\gamma M}{A_p + A} A + \eta U - \delta A, & \text{(26b)} \\ \dfrac{dU}{dt} = \nu \dfrac{\gamma M}{A_p + A} A - \eta U - \delta U. & \text{(26c)} \end{cases}$$

Following the same rationale as in Section 3.1, it is straightforward to show that system (25) admits two equilibria, $\mathbf{E}_0$, and $\mathbf{E}^*_{1,P} = (M^*_{1,P}, A^*_{1,P}, U^*_{1,P})$, where $A^*_{1,P}$ is the positive root of the quadratic equation

$$\left(\frac{\delta+\nu+\eta}{\delta+\eta}\right)\left(\frac{(1-r)\mu+\delta r}{1-r}\right)A^2 + \left[\left(\frac{\delta r}{1-r}+(\mu+\alpha)\right)\left(\frac{\delta+\nu+\eta}{\delta+\eta}\right)A_p - \frac{\mu}{\sigma}\ln\mathcal{N}_F\right]A - (\mu+\alpha)A_p\frac{1}{\sigma}\ln\mathcal{N}_F = 0,$$

or, after simplification,

$$\left(\frac{\delta+\nu+\eta}{\delta+\eta}\right)\left(\frac{\vartheta}{1-r}\right)A^2 + \left[\left(\frac{\vartheta}{1-r}+\alpha\right)\left(\frac{\delta+\nu+\eta}{\delta+\eta}\right)A_p - \frac{\mu}{\sigma}\ln\mathcal{N}_F\right]A - (\mu+\alpha)A_p\frac{1}{\sigma}\ln\mathcal{N}_F = 0.$$

Notably, the above equation has only one positive real root because its discriminant is positive, the branches of the corresponding parabola are directed upwards, while its cross with the vertical axis is negative. By setting Δ as the discriminant of the above quadratic equation, we deduce

$$A^*_{1,p} = \frac{1}{2\left(\frac{\delta+\nu+\eta}{\delta+\eta}\right)\left(\frac{(1-r)\mu+\delta r}{1-r}\right)}\left[\frac{\mu}{\sigma}\ln\mathcal{N}_F - \left(\frac{r}{1-r}+(\mu+\alpha)\right)\left(\frac{\delta+\nu+\eta}{\delta+\eta}\right)A_p + \sqrt{\Delta}\right], \quad \text{(27a)}$$

$$U^*_{1,p} = \frac{\nu}{\delta+\eta}A^*_{1,P}, \quad \text{(27b)}$$

$$M^*_{1,p} = \frac{r\rho}{\mu + \alpha\dfrac{A_p}{A^*_{1,P}+A_p}}\frac{1}{\mathcal{N}_F}\frac{\nu}{\delta+\eta}A^*_{1,P}. \quad \text{(27c)}$$

Note also that $M^*_{1,p} + A^*_{1,p} + U^*_{1,p} = \frac{1}{\sigma}\ln\mathcal{N}_F$, indicating that in the male abundance case, there is no impact on the total population. Of course, when $A_p = 0$, we recover the positive equilibrium $\mathbf{E}^*_1$ given by (15) in Section 3.1.

Last but not least, following the same methodology as in Appendix A, it is straightforward to show that for system (25), we have the following result.

Proposition 4. *Consider the ODE system (25) with $A_p \geq 0$ and $\alpha \in [0,1]$. Then the following statements are valid:*

(i) *If $\mathcal{N}_F < 1$, the trivial equilibrium $\mathbf{E}_0$ is LAS.*

(ii) *If $\mathcal{N}_F > 1$, a strictly positive equilibrium $\mathbf{E}^*_{1,p}$ defined by (27) is LAS and $\mathbf{E}_0$ is unstable; however, there always exists a trajectory converging to $\mathbf{E}_0$ meaning that $\mathbf{E}_0$ is not a repeller.*

Remark 2. It is expected that $\mathbf{E}^*_{1,p}$ defined by (27) will be a virtual equilibrium of the continuous PWS system (24) even for relatively small values of $\alpha \in [0,1]$ and $A_p > 0$. Even if the initial condition satisfies the relationship $\gamma M_0 > A_0$, positive values of α will cause a decrease in the current value of $M(t)$, while positive values of A_p will force the mating function to drop below the unity value thus enabling the trajectories of the PWS system (24) to cross the switching plane $\widetilde{\mathcal{P}}_s(A_p)$ at relatively small $t \geq 0$. The latter will imply that the subsystem (26) will become active.

Let us now focus on system (26). Like in Section 3.2, it is straightforward to show that $\mathbf{E}_0$ is still an equilibrium. However, mating disrupting entails the Allee effect when the system parameters correspond to the male-scarcity case. Namely, $\mathbf{E}_0$ may remain locally asymptotically stable as long as *a sufficient amount of* pheromones are released and regardless of $\mathcal{N}_F$. The latter can be shown via direct computation of the Jacobian matrix at equilibrium $\mathbf{E}_0$. This property is essential because it allows the use of a small amount of pheromones to control a non-established population and, from the field application point of view, to derive a massive and small releases strategy, like in the Sterile Insect Technique [46]. Notwithstanding, showing the existence of at least one positive equilibrium for system (26) is a bit more complicated than in Section 3.2.

Proposition 5. *Consider the ODE system (26) with $A_p \geq 0, \alpha \in [0,1]$ and assume that $\theta_M > 1$, where θ_M is defined by (17). Then, for each fixed $\alpha \in [0,1]$, there exists a threshold quantity $A_p^{crit} > 0$ such that the following statements are valid:*

(i) *When $0 < A_p < A_p^{crit}$, system (26) admits 2 positive equilibria, $\mathbf{E}_{1,p}$ and $\mathbf{E}_{2,p}$.*

(ii) *When $A_p = A_p^{crit}$, system (26) admits only one positive equilibrium $\mathbf{E}_{*,p}$.*

(iii) *When $A_p > A_p^{crit}$, system (26) has no positive equilibrium.*

Proof. The full and detailed proof is given in Appendix B . Here, we only provide a practical outlook for finding the threshold value A_p^{crit} corresponding to a fixed $\alpha \in [0,1]$. An algebraic system consisting of two nonlinear equations (see Eq. (B.6) in Appendix B) renders as solution the value of A_p^{crit} and the coordinate $A_{*,p}$ of the equilibrium $\mathbf{E}_{*,p}$ (mentioned in item **(ii)**) of the ODE system (26) with A_p replaced by A_p^{crit} and the same fixed $\alpha \in [0,1]$. The other two coordinates $M_{*,p}$ and $U_{*,p}$ of $\mathbf{E}_{*,p}$ can be calculated using formulas (B.3) and (B.4) given in Appendix B. Then, if we choose $0 < A_p < A_p^{crit}$ for the same fixed $\alpha \in [0,1]$ and substitute them into (B.5) we can find the coordinates $A_{i,p}, i = 1,2$ of the two equilibria $\mathbf{E}_{i,p}, i = 1,2$ of the system (26) (mentioned in item **(i)**), whose other two coordinates $M_{i,p}$ and $U_{i,p}, i = 1,2$ can be found by (B.3) and (B.4) given in Appendix B. However, if we choose $A_p > A_p^{crit}$ for the same fixed $\alpha \in [0,1]$ and substitute them into Eq. (B.5), we obtain no solution (see Fig. B.1 in Appendix B), meaning that item **(iii)** is applicable. ■

From Proposition 5, when $A_p > A_p^{crit}$, we deduce that the only equilibrium of the system (26) is $\mathbf{E}_0$, which is always LAS.

Remark 3. The previous result shows that massive releases of pheromones can be used to suppress or eradicate the ACP population. However, the emission of pheromones in large quantities is not always necessary as long as we can estimate the wild population during the intervention. That is why the closed-loop control approach can help derive some strategies relying on a minimal amount of pheromones. Section 4.2 addresses this issue in more detail.

It is also possible to show that $\mathbf{E}_0$ is not only LAS but also GAS (*globally asymptotically stable*) when A_p is sufficiently large. Following [21], it is easy to check that the right-hand side of system (26) is not quasi-monotone because of the term $-\nu \frac{\gamma M}{A_p + A} A$. However, it is possible to consider an auxiliary system that is monotone cooperative and provides an upper-bound for the solution of system (26) by removing $-\nu \frac{\gamma M}{A_p + A} A$ and also some exponential terms. The auxiliary system becomes

$$\begin{cases} \dfrac{dM}{dt} = r\rho U e^{-\sigma M} - \alpha \dfrac{A_p}{A_p + A} M - \mu M, & \text{(28a)} \\ \dfrac{dA}{dt} = (1-r)\rho U + \eta U - \delta A, & \text{(28b)} \\ \dfrac{dU}{dt} = \nu \dfrac{\gamma M}{A_p + A} A - \eta U - \delta U. & \text{(28c)} \end{cases}$$

We can derive the following result.

Proposition 6. *For the auxiliary system (28) with $A_p > 0$ and $\alpha \in [0,1]$, the following statements are valid:*

(a) *System (28) defines a positive dynamical system on $\mathbb{R}^3_+$.*

(b) *The trivial equilibrium $\mathbf{E}_0 = \mathbf{0}$ of the system (28) is always LAS.*

(c) *There exists $\tilde{A}_p^{crit} > 0$ such that*

(i) *If $A_p > \tilde{A}_p^{crit}$, then $\mathbf{E}_0 = \mathbf{0}$ is GAS on $\mathbb{R}^3_+$.*

(ii) *If $0 < A_p < \tilde{A}_p^{crit}$, system (28) admits two positive equilibria $\tilde{\mathbf{E}}_{1,p}$ and $\tilde{\mathbf{E}}_{2,p}$ such that $\tilde{\mathbf{E}}_{1,p} < \tilde{\mathbf{E}}_{2,p}$. Moreover, the basin of attraction of $\mathbf{E}_0$ contains the set $\left\{\mathbf{X} \in \mathbb{R}^3_+ : \mathbf{E}_0 \leq \mathbf{X} < \tilde{\mathbf{E}}_{1,p}\right\}$, and the basin of attraction of $\tilde{\mathbf{E}}_{2,p}$ contains the set $\left\{\mathbf{X} \in \mathbb{R}^3_+ : \mathbf{X} \geq \tilde{\mathbf{E}}_{2,p}\right\}$.*

Proof. See Appendix C □

Finally, by comparison (see, e.g., [47]), any solution of (28) is an upper bound for the solution of (26) with the same initial point. This implies that the basin of attraction of $\mathbf{E}_0$ as an equilibrium of (26) contains the sets given in Proposition 6(c). Thus we deduce the following statement.

Theorem 1. *For the ODE system (26) with $A_p > 0$ and $\alpha \in [0,1]$, the following statements are valid:*

(a) *If $0 < A_p < \tilde{A}_p^{crit}$, the basin of attraction of $\mathbf{E}_0$ contains the set $\left\{\mathbf{X} \in \mathbb{R}^3_+ : \mathbf{E}_0 \leq \mathbf{X} < \tilde{\mathbf{E}}_{1,p}\right\}$.*

(b) *If $A_p > \tilde{A}_p^{crit}$, then $\mathbf{E}_0 = \mathbf{0}$ is GAS on $\mathbb{R}^3_+$.*

Remark 4. From Proposition 6 it stems that, by comparison, if $A_p > \tilde{A}_p^{crit}$ then the solution of the auxiliary system (28) will converge to $\mathbf{E}_0 = \mathbf{0}$. Therefore, again by comparison, the trajectories of the ODE system (26) will also converge to $\mathbf{E}_0 = \mathbf{0}$ for any initial condition $(M_0, A_0, U_0) \in \mathbb{R}^3_+$. Thus, in full generality, we have that A_p^{crit} that appears in Proposition 5 fulfills the condition $A_p^{crit} < \tilde{A}_p^{crit}$.

To illustrate the results of Proposition 5 and Theorem 1, let us consider the PWS system (1) describing the natural ACP dynamics with parameter values defined in Table 1 that fulfill the relationship $\mathcal{N}_M > \mathcal{N}_F > 1$ (see more details at the beginning of Section 5). Suppose that the ACP population is well established, meaning that the population size is close $\mathbf{E}^*_1$ defined by (15), which is a regular LAS equilibrium. Now let pass to the controlled PWS system (24) with initial condition $(M_0, A_0, U_0) = \mathbf{E}^*_1$ where $\alpha \in [0,1]$ and $A_p > 0$. We can assess the threshold value A_p^{crit} for any fixed α using the technique described in

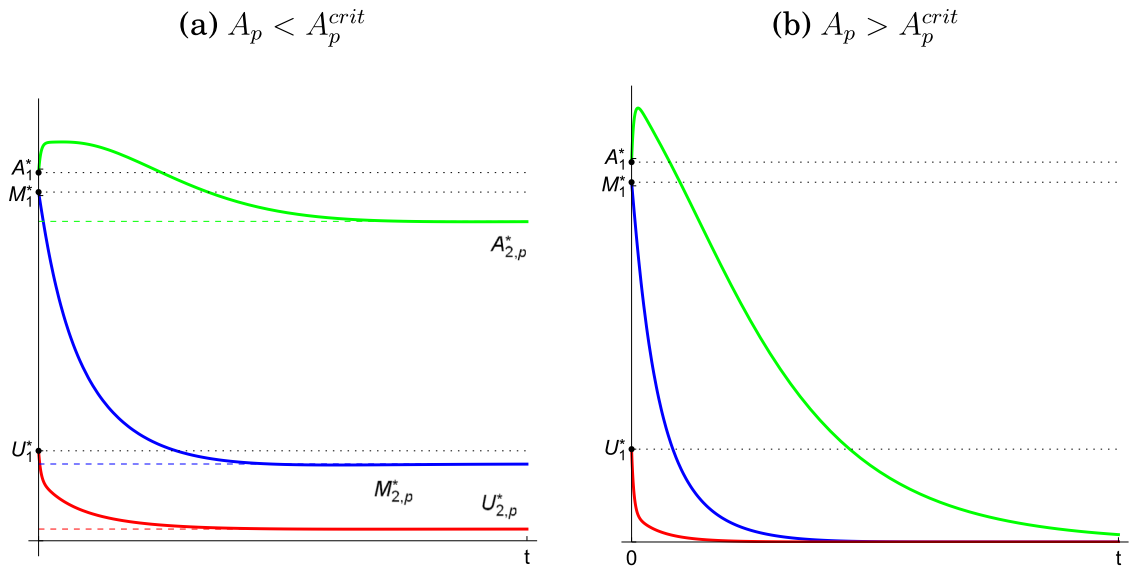

Fig. 7. Open-loop control of well-established ACP population: (a) suppression of the population $\left(M(t), A(t), U(t)\right) \to \tilde{\mathbf{E}}_{2,p}^*$ where $\mathbf{E}_{2,p}^* < \mathbf{E}_1^*$; (b) elimination of the population $\left(M(t), A(t), U(t)\right) \to \mathbf{E}_0$.

Appendix B. For example, when $\alpha = 0.1$, we have $A_p^{crit} \approx 1805$. Thus, by choosing $A_p < A_p^{crit}$ only a suppression of the initial population can be reached meaning that the trajectories of PWS system (24) will converge to $\mathbf{E}_{2,p}^* = \left(M_{2,p}^*, A_{2,p}^*, U_{2,p}^*\right)$ such that $\mathbf{E}_{2,p}^* < \mathbf{E}_1^*$ (see chart (a) in Fig. 7). However, if we choose $A_p > A_p^{crit}$, the ACP population can be eliminated. In this case, the trajectories of PWS system (24) will converge to $\mathbf{E}_0$ as shown in the chart (b) in Fig. 7. Ultimately, Fig. 7 also confirms that the PWS system (24) is expected to behave like its male-scarcity subsystem (26) even for small $A_p < A_p^{crit}$ and despite that, before the beginning of control, the natural ACP dynamics exhibited the abundance of males, i.e., $\mathcal{N}_M > \mathcal{N}_F > 1$ (see Remark 2).

Thus, Theorem 1 provides the following helpful information from the practical perspective to control well-established ACP populations:

- As long as $A_p < A_p^{crit}$, an established ACP population can only be suppressed.
- An established ACP population can only be eliminated when $A_p > A_p^{crit}$.

However, an invading or non-established population with an initial condition $\left(M_0, A_0, U_0\right) < \tilde{\mathbf{E}}_{1,p}^*$ can be eradicated even by choosing $A_p < A_p^{crit}$.

4.2. Closed-loop control approach

Let us now assume that the total amount of sex pheromones expressed in terms of "false" females is proportional to the number of natural female psyllids $A(t)$ seeking for mating that is,

$$A_p = k \times A(t), \tag{29}$$

where the constant $k > 0$ defines the "gain" of feedback. Then, in the male-abundance region $\gamma M > A + A_p = (k+1)A$, the dynamical system (24) takes the following form:

$$\begin{cases} \dfrac{dM}{dt} = r\rho U e^{-\sigma(M+A+U)} - \alpha \dfrac{k}{k+1} M - \mu M, & \text{(30a)} \\ \dfrac{dA}{dt} = (1-r)\rho U e^{-\sigma(M+A+U)} - \nu A + \eta U - \delta A, & \text{(30b)} \\ \dfrac{dU}{dt} = \nu A - \eta U - \delta U. & \text{(30c)} \end{cases}$$

Alternatively, in the male-scarcity region $\gamma M < A + A_p = (k+1)A$, the dynamical system (24) becomes

$$\begin{cases} \dfrac{dM}{dt} = r\rho U e^{-\sigma(M+A+U)} - \alpha \dfrac{k}{k+1} M - \mu M, & \text{(31a)} \\ \dfrac{dA}{dt} = (1-r)\rho U e^{-\sigma(M+A+U)} - \dfrac{\gamma\nu}{k+1} M + \eta U - \delta A, & \text{(31b)} \\ \dfrac{dU}{dt} = \dfrac{\gamma\nu}{k+1} M - \eta U - \delta U. & \text{(31c)} \end{cases}$$

Let us now derive, for both systems (30) and (31), the conditions that define either the permanence or extinction of the ACP population under the feedback (29) and in the presence of male-killing traps. To do so, we will employ the next-generation approach initially derived for epidemiological systems [48] and later adapted to more general population dynamics models, see for instance [41,49]. This approach consists in determining the spectral radius of the next-generation matrix evaluated in the trivial equilibrium of the population dynamics model. To construct the next-generation matrix, the right-hand side of the dynamical system is written in the form

$$\frac{d\mathbf{X}}{dt} = \mathbf{G}(\mathbf{X}) := \mathcal{F}(\mathbf{X}) - \mathcal{V}(\mathbf{X}),$$

where the vector $\mathcal{F}(\mathbf{X})$ gathers all terms dealing with the emergence of new individuals, while the vector $\mathcal{V}(\mathbf{X})$ contains the transition and mortality terms. For the systems (30) and (31), the vector $\mathcal{F}(\mathbf{X})$ is same, that is,

$$\mathcal{F}(\mathbf{X}) = \begin{pmatrix} r\rho\, U e^{-\sigma(M+A+U)} \\ (1-r)\rho\, U e^{-\sigma(M+A+U)} \\ 0 \end{pmatrix}, \qquad \mathbf{X} = \begin{pmatrix} M \\ A \\ U \end{pmatrix},$$

while $\mathcal{V}(\mathbf{X})$ takes different forms:

$$\text{System (30)} \Rightarrow \mathcal{V}(\mathbf{X}) = \mathcal{V}_1(\mathbf{X}) = \begin{pmatrix} \dfrac{\alpha k}{k+1} M + \mu M \\ (\nu+\delta)A - \eta U \\ (\eta+\delta)U - \nu A \end{pmatrix},$$

$$\text{System (31)} \Rightarrow \mathcal{V}(\mathbf{X}) = \mathcal{V}_2(\mathbf{X}) = \begin{pmatrix} \dfrac{\alpha k}{k+1} M + \mu M \\ \dfrac{\gamma\nu}{k+1} M + \delta A - \eta U \\ (\eta+\delta)U - \dfrac{\gamma\nu}{k+1} M \end{pmatrix}.$$

The next step is to calculate the Jacobian matrices of $\mathcal{F}, \mathcal{V}_i, i = 1, 2$ and evaluate them in the trivial equilibrium $\mathbf{E}_0 = (0, 0, 0)$:

$$F := \frac{\partial \mathcal{F}}{\partial \mathbf{X}}\Big|_{\mathbf{E}_0} = \begin{pmatrix} 0 & 0 & r\rho \\ 0 & 0 & (1-r)\rho \\ 0 & 0 & 0 \end{pmatrix},$$

$$V_1 := \frac{\partial \mathcal{V}_1}{\partial \mathbf{X}}\Big|_{\mathbf{E}_0} = \begin{pmatrix} \frac{\alpha k}{k+1}+\mu & 0 & 0 \\ 0 & \nu+\delta & -\eta \\ 0 & -\nu & \eta+\delta \end{pmatrix},$$

$$V_2 := \frac{\partial \mathcal{V}_2}{\partial \mathbf{X}}\Big|_{\mathbf{E}_0} = \begin{pmatrix} \frac{\alpha k}{k+1}+\mu & 0 & 0 \\ \frac{\gamma\nu}{k+1} & \delta & -\eta \\ -\frac{\gamma\nu}{k+1} & 0 & \eta+\delta \end{pmatrix}.$$

Subsequently, the next-generation matrices of the form $FV_i^{-1}, i = 1, 2$ can be constructed for the dynamical systems (30) and (31), and their respective eigenvalues can be identified. Let us start by constructing the next-generation matrix for the system (30):

$$FV_1^{-1} = \begin{pmatrix} 0 & 0 & r\rho \\ 0 & 0 & (1-r)\rho \\ 0 & 0 & 0 \end{pmatrix} \begin{pmatrix} \frac{k+1}{k(\alpha+\mu)+\mu} & 0 & 0 \\ 0 & \frac{\delta+\eta}{\delta(\delta+\eta+\nu)} & \frac{\eta}{\delta(\delta+\eta+\nu)} \\ 0 & \frac{\nu}{\delta(\delta+\eta+\nu)} & \frac{\delta+\nu}{\delta(\delta+\eta+\nu)} \end{pmatrix}$$

$$= \begin{pmatrix} 0 & \frac{r\rho\nu}{\delta(\delta+\eta+\nu)} & \frac{r\rho(\delta+\nu)}{\delta(\delta+\eta+\nu)} \\ 0 & \frac{(1-r)\rho\nu}{\delta(\delta+\eta+\nu)} & \frac{(1-r)\rho(\delta+\nu)}{\delta(\delta+\eta+\nu)} \\ 0 & 0 & 0 \end{pmatrix}.$$

The next-generation matrix FV_1^{-1} corresponding to the dynamical system (30) is upper-triangular, and its eigenvalues are located on the main diagonal. There are two zero eigenvalues ($\lambda_1^{(1)} = \lambda_3^{(1)} = 0$) and a positive one that determines the spectral radius of FV_1^{-1}:

$$\lambda_2^{(1)} = \frac{(1-r)\rho\nu}{\delta(\delta+\eta+\nu)} = \mathcal{N}_F > 0.$$

Thus, the spectral radius of the next-generation matrix FV_1^{-1} corresponding to the dynamical system (30) does not depend on the control parameters k and α. Moreover, the spectral radius of FV_1^{-1} is precisely the basic offspring number $\mathcal{N}_F$ related to the female population of psyllids, which was already derived for the dynamical system (3)–(4) describing the natural ACP dynamics under the male abundance (cf. formula (9)).

Furthermore, following Section 3.1, replacing $-\mu$ by $-\mu + \alpha\frac{k}{k+1}$, and using similar computations to those developed in Appendix A, one can deduce that there exists a strictly positive equilibrium $\mathbf{E}_{1,P}^* \leq \mathbf{E}_1^*$ whose coordinates are

$$M_{1,P}^* = \frac{(k+1)r\delta}{(k+1)r\delta + \big(\alpha k + (k+1)\mu\big)(1-r)} \frac{1}{\sigma} \ln \mathcal{N}_F, \tag{32a}$$

$$A_{1,P}^* = \frac{(\eta+\delta)(1-r)}{\nu+\eta+\delta} \frac{\alpha k + (k+1)\mu}{(k+1)r\delta + \big(\alpha k + (k+1)\mu\big)(1-r)} \frac{1}{\sigma} \ln \mathcal{N}_F, \tag{32b}$$

$$U_{1,P}^* = \frac{\nu(1-r)}{\nu+\eta+\delta} \frac{\alpha k + (k+1)\mu}{(k+1)r\delta + \big(\alpha k + (k+1)\mu\big)(1-r)} \frac{1}{\sigma} \ln \mathcal{N}_F. \tag{32c}$$

When $\alpha = 0$ or $k = 0$, we recover the equilibrium $\mathbf{E}_1^*$ given by (15). Then, we derive the following result.

Proposition 7. *Consider the ODE system with feedback (29) defined by (30). Then the following statements are valid:*

(i) *If $\mathcal{N}_F < 1$, the trivial equilibrium $\mathbf{E}_0$ is LAS.*

(ii) *If $\mathcal{N}_F > 1$, a strictly positive equilibrium $\mathbf{E}_{1,P}^*$ defined by (32) is LAS, and $\mathbf{E}_0$ is unstable.*

Remark 5. It is interesting to notice that trapping alone is insufficient to suppress the pest population drastically. When $\alpha = 0$ while $A_p = kA(t) > 0$ is small enough (meaning that the subsystem (30) is in action and the equilibrium $\mathbf{E}_{1,P}^*$ is regular), we have $\mathbf{E}_{1,P}^* = \mathbf{E}_1^*$ (cf. formulas (32) and (15)). Therefore, releasing a small amount of pheromones has absolutely no impact on the population.

Let us now construct the next-generation matrix for the system (31):

$$FV_2^{-1} = \begin{pmatrix} 0 & 0 & r\rho \\ 0 & 0 & (1-r)\rho \\ 0 & 0 & 0 \end{pmatrix} \begin{pmatrix} \frac{k+1}{k(\alpha+\mu)+\mu} & 0 & 0 \\ -\frac{\gamma\nu}{(\delta+\eta)\big(k(\alpha+\mu)+\mu\big)} & \frac{1}{\delta} & \frac{\eta}{\delta(\delta+\eta)} \\ \frac{\gamma\nu}{(\delta+\eta)\big(k(\alpha+\mu)+\mu\big)} & 0 & \frac{1}{\delta+\eta} \end{pmatrix}$$

$$= \begin{pmatrix} \frac{r\rho\gamma\nu}{(\delta+\eta)\big(k(\alpha+\mu)+\mu\big)} & 0 & \frac{r\rho}{\delta+\eta} \\ \frac{(1-r)\rho\gamma\nu}{(\delta+\eta)\big(k(\alpha+\mu)+\mu\big)} & 0 & \frac{(1-r)\rho}{\delta+\eta} \\ 0 & 0 & 0 \end{pmatrix}.$$

The next-generation matrix FV_2^{-1} corresponding to the dynamical system (31) has only one linearly independent row (or column), and therefore it possesses only one non-zero eigenvalue:

$$\lambda_1^{(2)} = \frac{r\rho\gamma\nu}{(\delta+\eta)\big(k(\alpha+\mu)+\mu\big)}, \qquad \lambda_2^{(2)} = \lambda_3^{(2)} = 0. \tag{33}$$

Notably, this positive eigenvalue, which defines the spectral radius of the next-generation matrix FV_2^{-1}, depends on the control parameters k and α. Let us now recall that the spectral radius of FV_2^{-1} expresses the mean number of descendants produced by one individual during its lifetime and defines the basic offspring number for the dynamical system (31), that is,

$$\widetilde{\mathcal{N}}_M(k, \alpha) := \frac{r\rho\gamma\nu}{(\delta+\eta)\big(k(\alpha+\mu)+\mu\big)}. \tag{34}$$

It is worthwhile to point out that $\widetilde{\mathcal{N}}_M(k, \alpha) = \mathcal{N}_M$ only if $k = 0$ (no feedback); otherwise, we have $\widetilde{\mathcal{N}}_M(k, \alpha) < \mathcal{N}_M$, where $\mathcal{N}_M$ denotes the basic offspring number corresponding to the dynamical system (3)–(5) describing the natural ACP dynamics under the male scarcity (cf. formula (9)).

Let us also recall that the fulfillment of condition $\widetilde{\mathcal{N}}_M(k, \alpha) < 1$ would guarantee a local extinction of the ACP population described by the dynamical system (31). Therefore, one may choose the values of parameters $k > 0$ and $\alpha \in [0, 1]$ to satisfy this condition, namely

$$k > k^*(\alpha) = \frac{\mu(\mathcal{N}_M - 1)}{\alpha + \mu}, \tag{35}$$

where $k^*(\alpha)$ is a curve decreasing with respect to $\alpha \in [0, 1]$. Thus, we have established that the feedback gain $k > 0$ in (29) should satisfy the condition (35) in order to guarantee a local extinction of the ACP population.

Similarly to the male-abundance model, we can show the existence of a positive equilibrium, $\mathbf{E}_{2,P}^*$, for the male-scarcity model (31). Following Section 3.2, a straightforward computation leads to

$$M_{2,P}^* + A_{2,P}^* + U_{2,P}^* = \frac{1}{\sigma} \ln \widetilde{\mathcal{N}}_M(k, \alpha). \tag{36}$$

This equality is meaningful only when $\widetilde{\mathcal{N}}_M(k, \alpha) > 1$, that is

$$k < k^*(\alpha) = \frac{\mu(\mathcal{N}_M - 1)}{\alpha + \mu}, \tag{37}$$

which is exactly the opposite of (35). Further computations show that

$$A_{2,P}^* = \left(\frac{(1-r)\rho}{\delta} \frac{(\alpha+\mu)k + \mu}{\mu\mathcal{N}_M} - 1 \right) U = \big(\widetilde{\theta}_M(k, \alpha) - 1\big)U$$

exists if and only if $\widetilde{\theta}_M(k,\alpha) = \dfrac{(1-r)\rho}{\delta}\dfrac{1}{\widetilde{\mathcal{N}}_M(k,\alpha)} > 1$. In fact, since $\theta_M = \widetilde{\theta}_M(0,0) > 1$, and $\widetilde{\theta}_M(k,\alpha)$ being an increasing function of k and α, we deduce that $\widetilde{\theta}_M(k,\alpha) > 1$, for all $k \geq 0, \alpha \in [0,1]$ satisfying the condition $\widetilde{\mathcal{N}}_M(k,\alpha) > 1$. Furthermore, the coordinates of $\mathbf{E}^*_{2,P}$ have a form similar to (22) with θ_M and $\mathcal{N}_M$ replaced by $\widetilde{\theta}_M(k,\alpha)$ and $\widetilde{\mathcal{N}}_M(k,\alpha)$, respectively.

Finally, using the same computations as in Appendix A, we derive the following result.

Theorem 2. *For the ODE system (31) with feedback (29) and assuming $\mathcal{N}_M > 1$, the following statements are valid:*

(i) *If $k > k^*(\alpha)$, then $\mathbf{E}_0$ is LAS.*

(ii) *If $k < k^*(\alpha)$ and $\theta_M > 1$, then $\mathbf{E}^*_{2,P}$ is LAS and $\mathbf{E}_0$ is unstable.*

Remark 6. The previous result shows that elimination is reachable if the proportion of the released pheromones is sufficiently large. Indeed, emitting an amount of pheromones proportionally to the number of female individuals available for mating (A) present at each time will avoid having the Allee effect and bistability (exhibited in the open-loop case, see Section 4.1) and also allow that $\mathbf{E}_0$ be reachable and LAS even when a gradually decreasing amount of pheromones is being released.

In the following section, we discuss the interplay between the choice of the strength of lure A_p, including the feedback gain k, and the male-killing rate α and provide illustrations of the open-loop and closed-loop approaches using numerical simulations.

5. Numerical simulations and discussion

Since some biological parameters of *D. Citri* may change (due to environmental conditions, the host trees, etc.), so we begin this section by conducting a global sensitivity analysis to identify the parameters that are most sensitive to the outputs of the model (1).

In Figs. 8, 9, and 10, we show the outcomes of LHS-PRCC sensitivity analysis, where LHS stands for Latin Hypercube Sampling and PRCC for Partial Rank Correlation Coefficient. The LHS-PRCC method provides mainly information about how the outputs are impacted if we increase (or decrease) the inputs of a specific parameter (see, for instance, [50] for further information). The analysis is accomplished on the time segment $[800, 1000]$, with the ranges of values for the parameters given in Table 2.

The LHS-PRCC analysis was performed for the variables M, A, and U using a uniform distribution. It is very interesting to compare the impact of the parameters on the considered variables. In fact, the three variables M, A, and U are sensitive to the same parameters σ, μ, ν, δ, η, and ρ: see Figs. 8, 9, and 10. However, the most significant parameter is σ, followed by the mortalities μ and δ (for males M and receptive females A) or by mating receptiveness η (for fertilized females U). The fertility ρ also plays an essential role for males and females available for mating A, while ρ is less important for fertilized females U compared to mating receptiveness η and (re)mating rate ν. Notably, the primary sex ratio r and the mating competitiveness of males γ show almost no effect on all three subpopulations M, A, and U.

For all PRCC analysis, we used the PCC function (R software [54]) and 1000 bootstrap replicates, with a probability level of 0.95 for (the bootstrap) confidence intervals.

All the consequent simulations are performed using the base parameter values given in Table 1 and corresponding to the field study performed on Valencia sweet orange tree (Citrus sinensis) with Rangpur lime (Citrus limonia) taken as a rootstock [36]. First, we calculate the basic offspring numbers $\mathcal{N}_M$ and $\mathcal{N}_F$ for the natural dynamics of *D. citri* (see formulas (9)) described by the PWS dynamical system (3)–(5):

$$\mathcal{N}_M = 37.4256, \qquad \mathcal{N}_F = 32.2013.$$

Thus, for the natural ACP dynamics, we have $\mathcal{N}_M > \mathcal{N}_F > 1$, meaning the abundance of males, so the population of adult psyllids evolves according to the subsystem (7) of the PWS system (3). However, as the ACP life traits have noticeable variability (see value ranges in Table 2) due to seasonality, environmental conditions, host tree species, or rootstock, the ACP populations may also exhibit scarcity of males in other geographical regions. Nonetheless, both control approaches developed in Section 4 are applicable under the abundance or scarcity of males.

In this section, let us assume that, at the initial time $t = 0$, the natural ACP population is close to its steady state $\mathbf{E}_1 \in \mathbb{M}_a$, that is,

$$M(0) = 1519 \approx M^*_1, \qquad A(0) = 1590 \approx A^*_1, \qquad U(0) = 383 \approx U^*_1.$$

In the sequel, we perform numerical simulations of the PWS system (24) with the initial conditions given above and the parameter values from Table 1 while varying the control parameters A_p and α. Even though a strict and direct validation of the control parameters A_p and α is unavailable, an exploratory approach with values chosen within biologically plausible bounds informed by studies on pheromone attraction and trap use [19,43,44] helps identify conditions under which pheromone-based control could be effective.

Thanks to Theorem 1 (see Section 4.1) formulated for the open-loop control approach and using the technique employed in Appendices B and C, we can estimate the critical amount of pheromones, A_p^{crit}, necessary to guarantee the convergence towards $\mathbf{E}_0 = \mathbf{0}$ for different values of α, the trapping killing rate, as a numerical solution to the nonlinear system (B.6) from Appendix B. The results are given in Fig. 11, where the extinction region ($A_p > A_p^{crit}$) is above the blue-colored curve. This figure shows a considerable difference between $\alpha = 0$ and $\alpha > 0$, meaning that pheromones alone will only control the population at a very high cost, while even small increases of α from zero will help reduce considerably the pheromone-related cost because $\alpha \in [0,1]$ and $A_p^{crit} > 0$ exhibit negative correlation. Of course, the duration to enter more or less rapidly in the basin of attraction of $\mathbf{E}_0 = \mathbf{0}$ will depend on the amount of pheromones released. Here, we can use either massive or small release strategies developed earlier for the Sterile Insect Technique approach [46].

In Fig. 12, we show the total amount of pheromones needed to reach elimination under the open-loop control approach where A_p is chosen above A_p^{crit}, i.e., $A_p = A_p^{crit} + A_{p,min}$, for different values of $A_{p,min}$. Each of the colored curves displayed in Fig. 12 gives the *total* amount of pheromones as a function of $\alpha \in [0,1]$, which will be needed to reach the elimination of the ACP population when the pheromones are emitted at a constant rate $A_p = A_p^{crit} + A_{p,min}$. Notably, this figure has a logarithmic vertical scale while the total amount of pheromones depends not only on the constant pheromone emission rate but also on the total intervention time leading to elimination of the ACP population, that is,

$$\text{Total pheromone amount} = \big(\text{constant emission rate } A_p\big) \times \big(t_{end} - t_{start}\big),$$

where t_{start} and t_{end} mark the times the intervention is started and ended, respectively. As expected, the lower $A_{p,min} > 0$, the lower the total pheromones amount, but the intervention becomes longer. Thus, there is a balance to be found between the amount of pheromones available for releasing and the duration of the treatment. This tendency is also confirmed by Fig. 13 that exhibits the level sets of minimum-time estimates for (nearly) reaching extinction when such time is considered as a function of α and A_p.

Fig. 13 shows that combining pheromones and trapping is also essential to lower the time needed to (nearly) reach elimination. To estimate such a time T, we used the condition

$$\Big\|\big(M(T), A(T), U(T)\big)\Big\|_\infty = \max\Big\{M(T), A(T), U(T)\Big\} < 10^{-1} = 0.1 \qquad (38)$$

that expresses mathematically the elimination of the ACP population at $t = T$. Thus, Fig. 13 exhibits the level sets of minimum-time

Table 2
Parameter intervals for the *D. citri* model (1).

Parameter	Description	Unit	Range of values	References
r	primary sex ratio	–	$[0.23, 0.5]$	[51]
ρ	mean no. of eggs produced by one female per day	day^{-1}	$[2, 22]$	[52]
σ	characteristic of eggs survival to the adult stage	$individual^{-1}$	$[0.0005, 0.05]$	assumed
μ	natural mortality rate for males	day^{-1}	$[1/74, 1/10.41]$	[53]
δ	natural mortality rate for females	day^{-1}	$[1/80.2, 1/13.77]$	[53]
γ	females fertilized by a single male	–	$[0.2, 2]$	–
ν	transfer rate from A to U	day^{-1}	$[1/8, 1/2]$	[31]
η	transfer rate from U to A	day^{-1}	$[1/14, 2]$	[31]

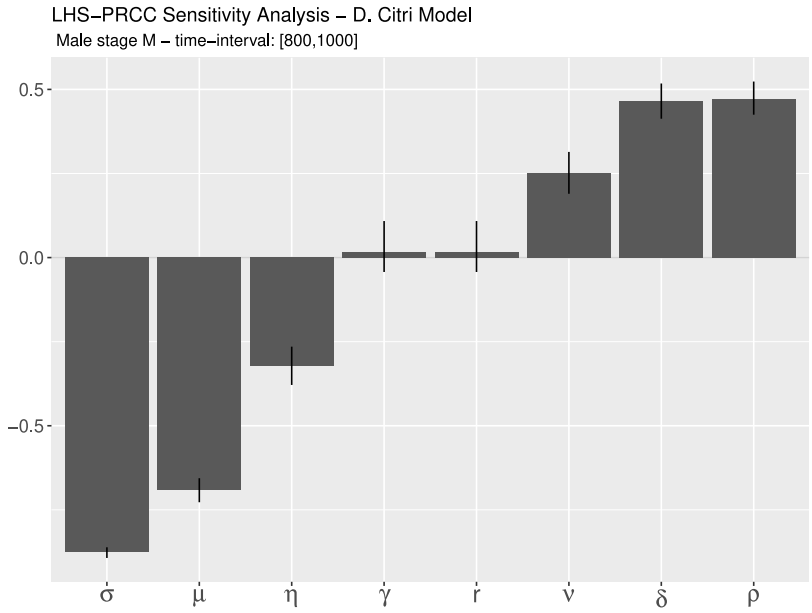

Fig. 8. LHS-PRCC Sensitivity analysis of the D. citri model - Males, M.

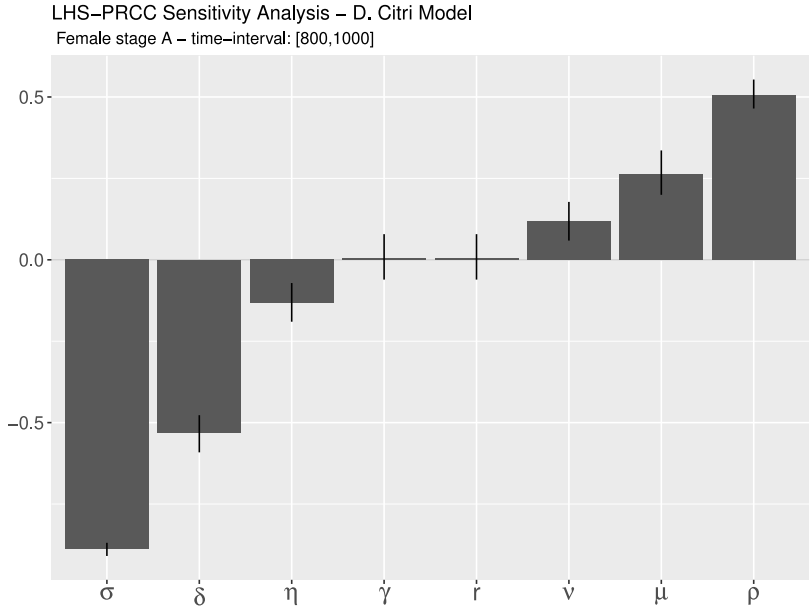

Fig. 9. LHS-PRCC Sensitivity analysis of the D. citri model - Mating Females, A.

estimates, T, for (nearly) reaching the population extinction when T is a numerical function of $\alpha \in [0, 1]$ and $A_p > 0$. In fact, the lowest time value is $T = 535$ days even if A_p is very large and α is close to 1. This is an interesting result because it shows that even if a sufficiently large value for A_p is available (to have $\mathbf{E}_0 = \mathbf{0}$ as a global attractor), using it in vast quantities will not be helpful. Of course, the larger α, the smaller

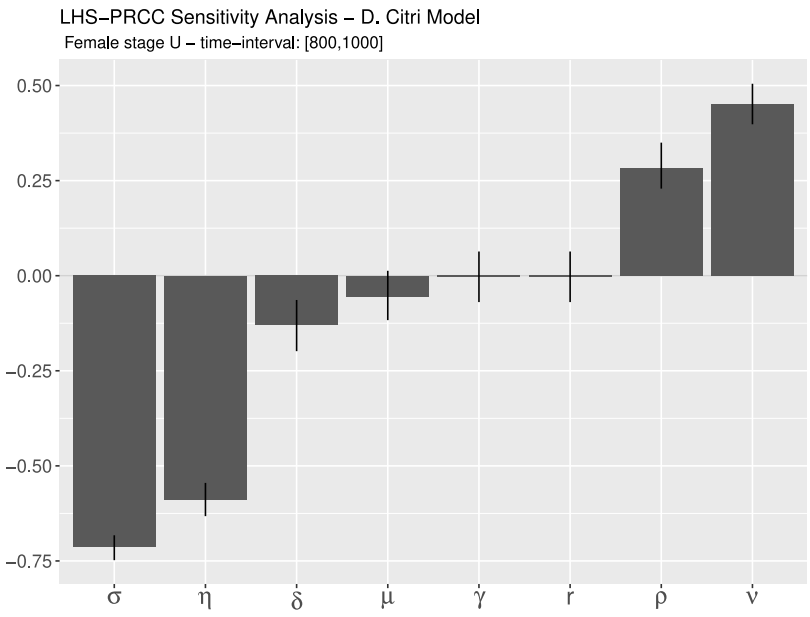

Fig. 10. LHS-PRCC Sensitivity analysis of the D. citri model - Fertile Females, U.

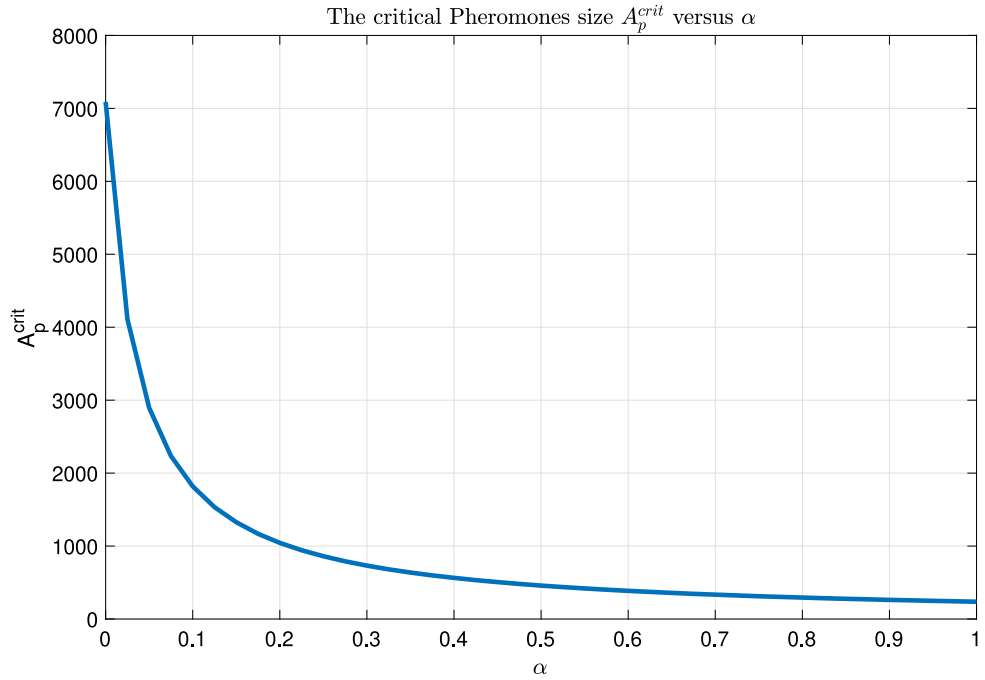

Fig. 11. Open-loop control. Numerical estimates of the critical pheromones amount, A_p^{crit}, versus α, the trapping killing rate, such that for all $A_p > A_p^{crit}$, the equilibrium $\mathbf{E}_0 = \mathbf{0}$ is GAS.

A_p: this shows that there is a tradeoff between these two quantities. If the trap has a certain fixed male-killing rate $\alpha \in [0, 1]$, then using Fig. 13, one may estimate the quantity of pheromones $A_p > 0$ to perform the intervention in an acceptable number of days T. Notably, there is no clear-cut way to affirm which parameter, α or A_p, is more efficient for controlling the ACP population, and a suitable tradeoff between α or A_p should be sought. In any case, it is deduced that releasing the pheromones alone is impractical.

Turning to the closed-loop control approach, Fig. 14 presents the plot of the curve $k^*(\alpha)$ (blue dotted line) that divides the positive quadrant into two regions. To plot this curve, we used formula (35) together with numerical values of parameters given in Table 1. The unshaded region below the curve $k^*(\alpha)$ contains all the values of k and α that guarantee only the suppression of the local ACP population because this is the case when $k < k^*(\alpha)$ meaning that $1 < \widetilde{\mathcal{N}}_M < \mathcal{N}_M$ (see formulas (9), (34)) and a positive equilibrium $\mathbf{E}_{2,P}$ satisfying the condition (36) exists. In contrast, the shaded region above the curve $k^*(\alpha)$ contains all the values of k and α that guarantee the elimination of the local ACP population because in this case we have $k > k^*(\alpha)$ and no positive equilibrium exists (see Theorem 2).

From Fig. 14, one may deduce that local elimination of the ACP population is possible even if $\alpha = 0$ (meaning that none of the male

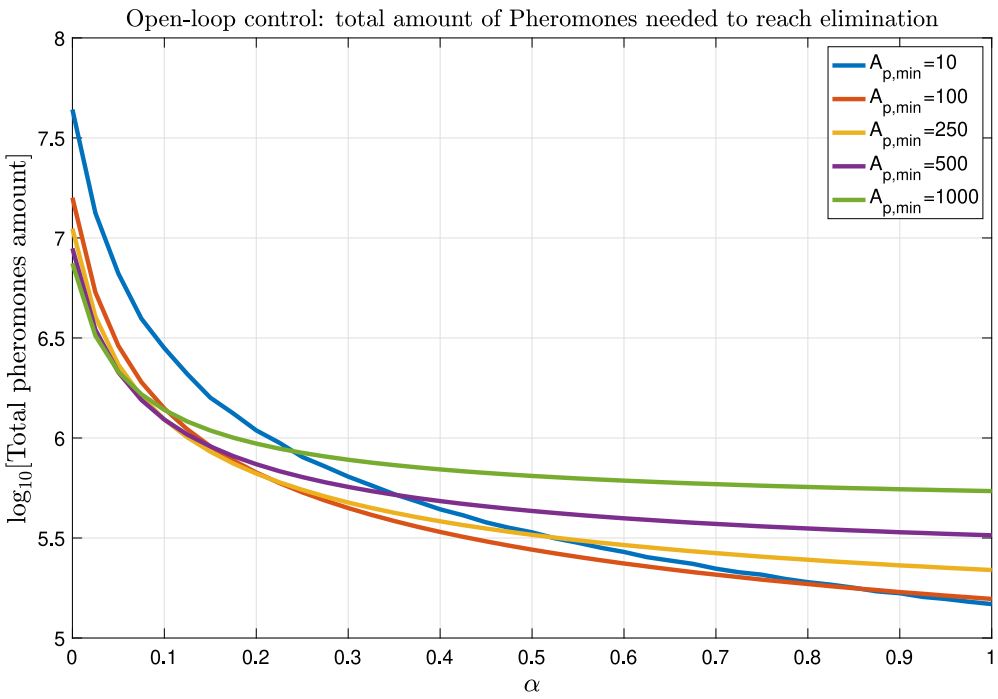

Fig. 12. Open-loop control. The total amount of pheromones needed to reach elimination of the ACP population for different values of $A_{p,min} > 0$ such that $A_p = A_p^{crit} + A_{p,min}$.

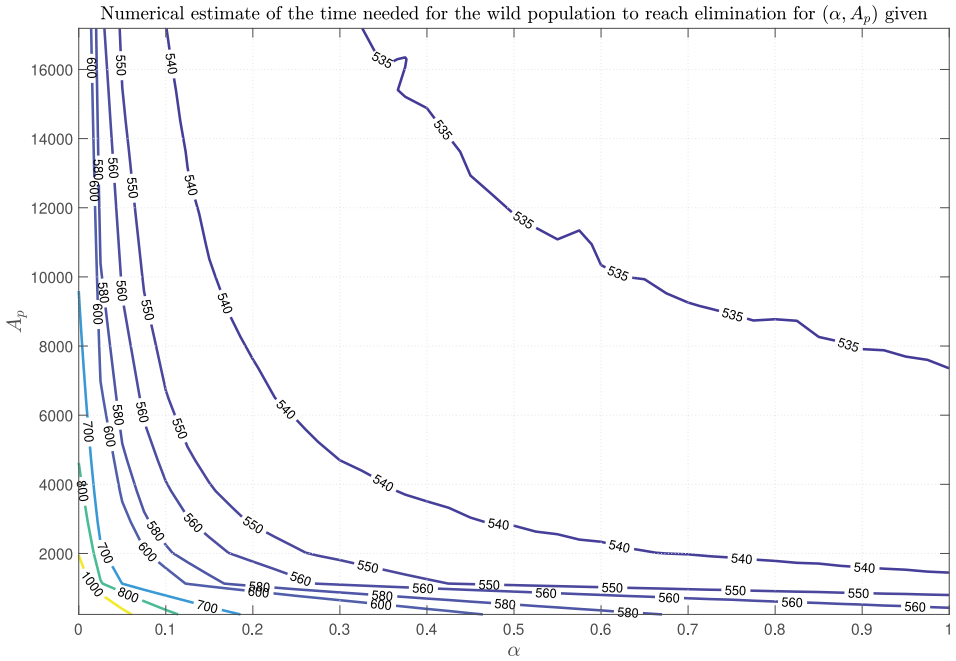

Fig. 13. Open-loop control. Estimates of minimal time T satisfying the condition (38) for (nearly) eliminating the ACP population, initially at equilibrium, with the trapping rate α and the amount A_p of released pheromones.

insects are killed when approaching or entering the trap). However, in such a case, the feedback gain k should be substantial ($k \geq 36.43$), meaning that a vast amount of sex pheromone should be emitted ($A_p \geq 36.43A(t)$, in terms of the "false" females). Fig. 14 also displays that the effect of male-killing rate α on the reduction of the total amount of sex pheromone needed is more visible for smaller values of α (below 50%) than for its larger values (above 50%). Nonetheless, even the traps with 100% male-killing rate ($\alpha = 1$) will still need a small feedback gain of about $k = 1$ ($A_p \geq A(t)$, in terms of the "false" females) to reach an eventual local elimination of *D. citri*.

Fig. 15 shows the evolution of the male M and female $F = A + U$ population in the phase plane (M, F) for different values of the male-killing rate α. Figs. 14 and 15 also illustrate Theorem 2 in the following sense. When the feedback gain is below the curve $k^*(\alpha)$ plotted in Fig. 14 (here we have chosen $k = 2.5$), we observe the convergence of the phase trajectories to the positive equilibrium $\mathbf{E}^*_{2,P}$ whose coordinates satisfy the condition (36), where $\widetilde{\mathcal{N}}_M > 1$ (see formula (34)). For

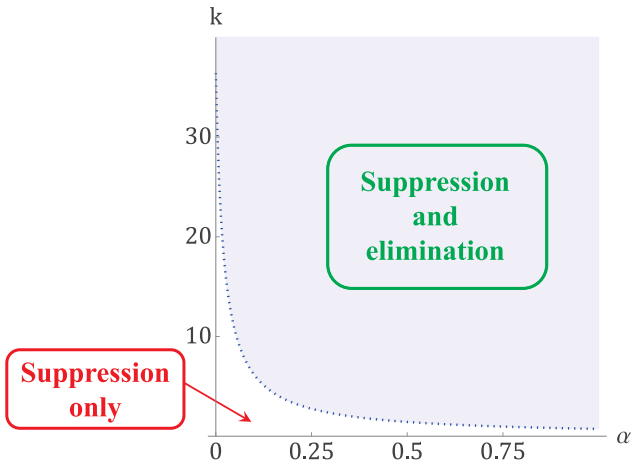

Fig. 14. Closed-loop control. The choice of the feedback gain k and male-killing rate α according to the condition (35).

different values of α, the corresponding $\mathbf{E}^*_{2,P}$ are marked by the black points on the left chart of Fig. 15. A thin black broken line on the left chart of Fig. 15 indicates the gradual changes in the position of $\mathbf{E}^*_{2,P}$ when α increases from 0.05 to 0.2 with a step of 0.05. Thus, the positive equilibrium $\mathbf{E}^*_{2,P}$ moves closer to the origin ($\mathbf{E}_0$) as α increases, but the population of males decays faster than that of females.

However, if the feedback gain is above the curve $k^*(\alpha)$ plotted in Fig. 14 (here we have chosen $k = \mathcal{N}_M$), we observe the convergence of the phase trajectories to the trivial equilibrium $\mathbf{E}_0$ (see the right chart in Fig. 15). Here, the density of males also decays faster than the density of females.

To compare the closed-loop and open-loop approaches, at least at the beginning of the pheromones treatment when the ACP population is close to its equilibrium value, we show the amount of pheromones needed to start the closed-loop control and the open-loop control: see Fig. 16. In this figure, the blue curve represents the estimates of the critical amount of pheromones, $A^*_{p,k} = k^*(\alpha) \times A^*_1$ as a function of $\alpha \in [0,1]$, such that for all $A_p > A^*_{p,k}$, the equilibrium $\mathbf{E}_0 = \mathbf{0}$ is GAS (closed-loop control). The red curve in Fig. 16 represents the estimates of the critical amount of pheromones, A^{crit}_p as a function of $\alpha \in [0,1]$, such that for all $A_p > A^{crit}_p$, the equilibrium $\mathbf{E}_0 = \mathbf{0}$ is GAS (open-loop control). Thus, contrasting these two curves, it is straightforward to see that the closed-loop control is very costly compared to the open-loop control, at least during the first weeks of the intervention. Indeed, the closed-loop control requires almost 9 times more pheromones than the open-loop control, regardless of the values for α. Also note that the red curve in Fig. 16 is the same as the blue one in Fig. 11 bearing a different scaling.

Notably, the result presented in Fig. 16 (blue curve) is somewhat idealistic because it corresponds to "continuous estimations" of the population size of female psyllids $A(t)$, available for mating, assuming that for all $t \geq 0$ the size of $A(t)$ can be accurately assessed. In practice, however, estimating the size of a local insect population can be a challenging and expensive task. Therefore, continuous population size estimations are unfeasible, and most IPM programs conduct such assessments with different frequencies varying from several weeks to several months [55], but not more often than every two weeks. Interested readers may learn more regarding practical methods for estimating wild insect populations in [56,57] or similar sources.

Using the closed-loop control approach, we have assessed the total amount of pheromones A_p (also for different values of the male-killing rate α) needed to reach elimination if the size of female psyllids available for mating, $A(t)$, is estimated every $2n$ weeks, where $n = 1, 2, \ldots, 6$. In Fig. 17, the vertical axis has a logarithmic scaling and the total quantity of pheromones is expressed by an integral taken over the total time T needed to reach the elimination of the ACP population, that is,

$$\text{Total pheromone amount} = \int_{t_{start}}^{T} A_p(t)dt.$$

Here, for the closed-loop control and each $\alpha \in [0,1]$, we have that $A_p(t) = \left(k^*(\alpha)+1\right) \times A\left(t_{2n\times j}\right)$ is piecewise constant, where $t_{2n\times j}$ with $j = 1, 2, \ldots$ denote the times when the wild population is estimated periodically until the condition (38) is met. In contrast, for the open-loop control, $A_p(t)$ is constant for each given $\alpha \in [0,1]$ and is defined as $A_p(t) = A^{crit}_p(\alpha) + A_{p,min}$ with $A_{p,min} = 100$. Fig. 17 shows that the closed-loop control performs better than the open-loop control. And, as expected, the smaller is n, the less is the total amount of pheromones for any $\alpha \in [0,1]$. However, we must be aware that estimating the population size in the field can be very difficult and also induces additional costs.

According to definition (29), closed-loop control becomes useful once the population is or has become small enough, meaning that $A_p = kA(t)$ is not too large. This rationale leads us to consider a mixed-type control and choose A_p, for instance, in the following way:

$$A_p = \min\left\{ A^{crit}_p(\alpha) + A_{p,min},\ \left(k^*(\alpha)+0.1\right)A(t^*) \right\}$$

with $A_{p,min} = 100$, for a given α, where $A(t^*)$ is an estimated value of A at a given time t^*. Like in the closed-loop case, we estimate the population size every $2n$ weeks, where $n = 1, 2, \ldots, 6$. Thus we choose

$$A_p(t_{2n\times j}) = \min\left\{ A^{crit}_p(\alpha) + 100,\ \left(k^*(\alpha)+0.1\right)A\left(t_{2n\times j}\right) \right\}, \qquad j = 1, 2, \ldots$$

and $n = 1, 2, \ldots, 6$. At the beginning of the treatment, it is expected that the open-loop control will need less pheromones than the closed-loop approach (see Fig. 16) until the ACP population reduces, at some finite time of estimation $t = t^*_{2n\times j}$, so that the relationship $A^{crit}_p(\alpha) > k^*(\alpha)A\left(t^*_{2n\times j}\right)$ will become valid. Then, starting from $t = t^*_{2n\times j}$, the closed-loop control will require emitting a smaller amount of pheromones than the open-loop constant control.

To illustrate this approach, we provide in Fig. 18, the total amount of pheromones, for different values of $\alpha \in [0,1]$, related to the estimates of the population size carried out every $2n$ weeks, where $n = 1, 2, \ldots, 6$. Note that Fig. 18 also has logarithmic scaling and the total amount of pheromones is defined in the integral form as indicated above. As expected, the mixed-type control is practical when α is large enough (compare with Fig. 12). Indeed, the mixed control regime requires a smaller amount of pheromones A_p for each given $\alpha \in [0,1]$ compared to solely open-loop or solely closed-loop regimes. This deduction is made visual by contrasting the colored curves in Figs. 17 and 18. However, one should also remember that the mixed control regime still requires to estimate the current ACP population sizes (every $2n$ weeks, $n = 1, \ldots, 6$) when the ACP population becomes relatively small compared to its initial size, and such estimation will generate extra costs. Altogether, the mixed-type control provides the best result in term of the rational use of the pheromone compounds, at least when $\alpha \geq 0.05$ and even for rather sparse frequencies (such as 12 weeks) of estimations of the wild population sizes.

6. Conclusions

Citrus fruits are among the most important crops worldwide, and many citrus cultures worldwide face the threat of HLB or citrus greening disease [3]. This disease is mainly transmitted by *D. citri*, an invasive psyllid species that colonizes citrus orchards in different parts of the world [1]. Controlling this pest population is a challenging task, and IPM programs are seeking environmentally friendly strategies that may replace the traditional ones based on pesticides. In this context, using pheromone traps seems rather promising because the attraction and direct removal of male insects induce mating disruption, thus reducing future offspring and suppressing the overall pest population.

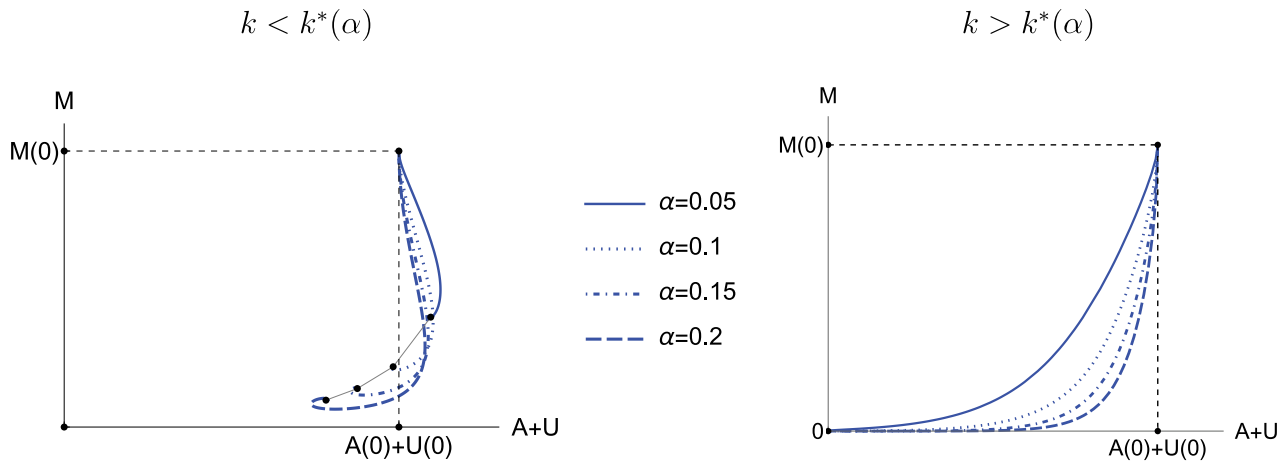

Fig. 15. Closed-loop control. The effect of male-killing rate α on the phase population trajectories of males M and females $F = A + U$ in the case of population suppression ($k < k^*(\alpha)$, *left chart*) and local elimination ($k > k^*(\alpha)$, *right chart*).

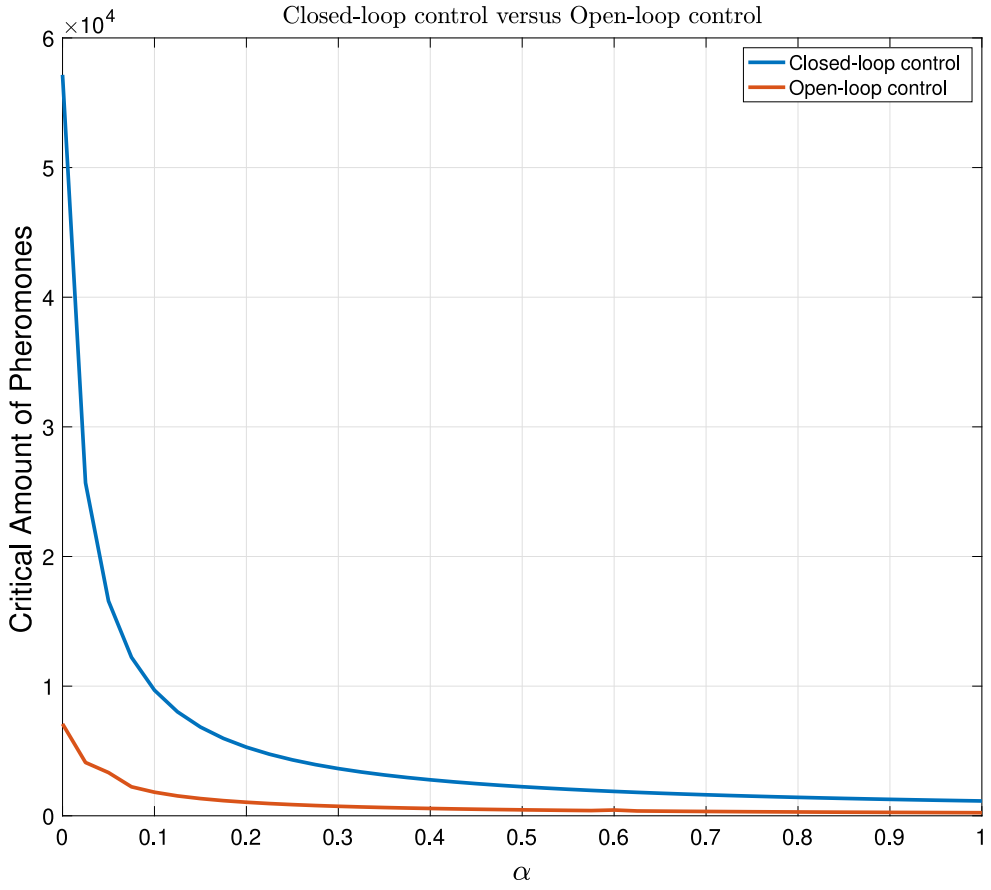

Fig. 16. Critical amount of pheromones at the beginning of the treatment for different male-killing rates $\alpha \in [0, 1]$ when using closed-loop control (blue curve) and open-loop control (red curve).

In this paper, we proposed and analyzed a model formulated as a piecewise smooth ODE system that describes the natural population dynamics of psyllids. This model was further amended with the external control actions, expressed by the parameters A_p (the strength of lure) and α (traps male-killing rate), to mimic the introduction of sex pheromone traps that enforce mating disruption and may lead either to the suppression or local extinction of the ACP population. From the theoretical standpoint, the choice of control parameters A_p and α, as well as their interplay, was conducted based on two operational control modes, the open-loop control approach (operating on a predefined sequence of actions) and the closed-loop control approach (whose actions can respond to changes in the system behavior). For both techniques, we have identified a critical curve or mapping, that is, A_p as a function of α, that plays the role of a threshold, below which only the ACP population suppression is achievable and above which the local pest extinction can be attained.

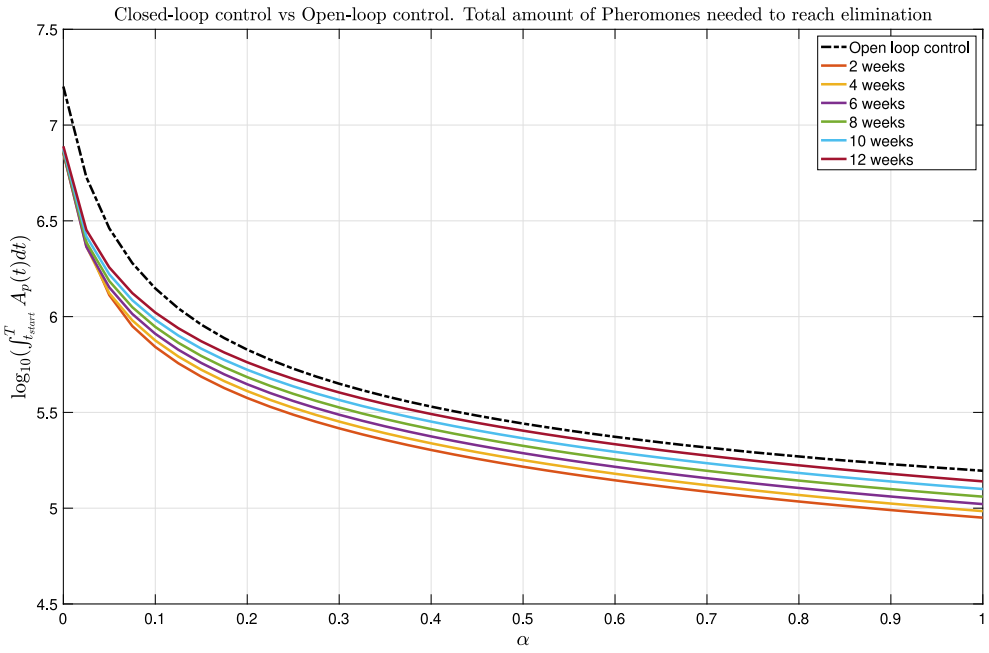

Fig. 17. Closed-loop control versus open-loop control, with $A_{p,\min} = 100$. Total amount of pheromones needed to reach elimination of the ACP population, when the population is estimated every $2n$ weeks, where $n = 1, 2..., 6$.

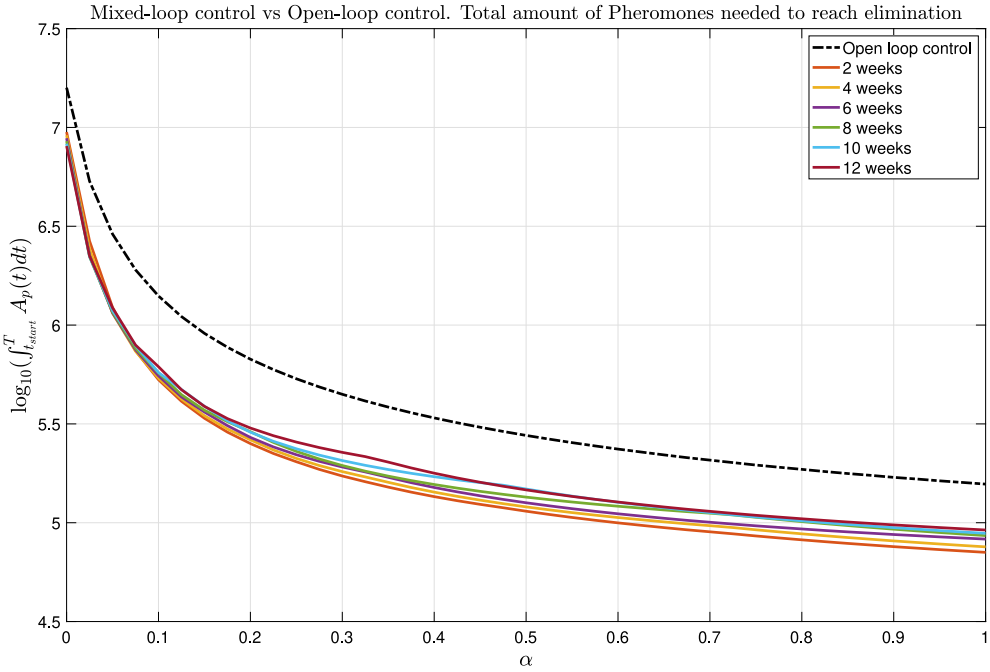

Fig. 18. Mixed-type control versus Open-loop control, with $A_{p,\min} = 100$. Total amount of pheromones needed to reach elimination of the ACP population under an "open-loop — closed-loop" control approach, when the population is estimated every $2n$ weeks, where $n = 1, 2..., 6$.

These theoretical findings also allowed us to perform qualitative *in silico* testings of the model and estimate not only the total amount of sex pheromones needed for the local elimination of the ACP population but also the minimum time to reach a local extinction of this pest. Compared to the numerical experiments performed in [20,21], our numerical results provide helpful information for the practical implementation of control by pheromone traps, such as the tradeoffs between three important metrics: the time needed to reach elimination of the pest, the total quantity of pheromones required for treatment, and the male-killing rate of the traps.

Summarizing the outcomes of the present work, we would like to highlight the following insight regarding the control of *D. citri* using the pheromone traps:

- Pheromone traps are a reliable alternative to pesticide use because they can suppress and even eliminate the ACP pest population while producing no harm to the crop.

- Releasing the pheromones alone without male-killing (i.e., with $\alpha = 0$) may also be employed to reach the final goal of pest population suppression or elimination. Nonetheless, it would require emitting a massive quantity of pheromones, while using male-killing traps would considerably reduce the pheromone quantity needed for controlling the pest population.
- Increasing the male-killing rate α of the traps may reduce the overall costs (i.e., the total amount of pheromones needed for intervention) and the time to reach elimination.
- Open-loop control strategies show better results when applied to established pest populations bearing large sizes. In contrast, closed-loop control strategies perform better for emerging populations or when the population is small. Thus, combining these two control approaches renders the best overall results and requires a smaller amount of pheromones.

It is worthwhile to point out that the model proposed in this paper lays solid grounds for combining the pheromone traps with other control intervention measures as a part of the IPM programs. In particular, a combination of the pheromone traps with the use of predators or parasitoids may render interesting results. The latter can also be tested to enhance the control efficiency against Huanglongbing, using a limited amount of pheromones, possibly by designing the optimal control strategies.

To reduce the total amount of pheromone, a metapopulation modeling involving the psyllid migration between treated and untreated trees may also be considered, for instance, by adapting an optimization approach developed in [58] or other relevant techniques. Furthermore, extensions of the present work may include the transmission of infection caused by *Candidatus* Liberibacter spp. and lead to the formulation and study of epidemiological models to reduce the risk of HLB spreading and its damage to citrus crops. All these potential perspectives lie beyond the scope of our present study, but they may be viewed as future research endeavors.

Finally, we hope that the outcomes of this study will provide valuable insights for developing alternatives to pesticides and also shed some light on the practical implementation of ecologically friendly pest management conducted in field trials.

CRediT authorship contribution statement

Daiver Cardona-Salgado: Writing – original draft, Software, Formal analysis, Visualization, Investigation. **Yves Dumont:** Writing – original draft, Writing – review & editing, Visualization, Methodology, Formal analysis, Software, Investigation, Conceptualization. **Olga Vasilieva:** Writing – original draft, Supervision, Investigation, Conceptualization, Writing – review & editing, Validation, Methodology, Formal analysis.

Declaration of competing interest

The authors declare the following financial interests/personal relationships which may be considered as potential competing interests: Olga Vasilieva reports financial support was provided by Colombia Ministry of Science Technology and Innovation. Yves Dumont reports financial support was provided by Conseil 1015 Regional de la Reunion. Yves Dumont reports financial support was provided by Conseil Departemental de la Reunion. Yves Dumont reports financial support was provided by Centre for International Cooperation in Agricultural Development Research. Daiver Cardona-Salgado reports financial support was provided by Colombia Ministry of Science Technology and Innovation. Yves Dumont reports financial support was provided by University of Pretoria. If there are other authors, they declare that they have no known competing financial interests or personal relationships that could have appeared to influence the work reported in this paper.

Acknowledgments

This research was funded by the National Fund for Science, Technology, and Innovation (Autonomous Heritage Fund *Francisco José de Caldas*) by way of the Research Program No. 1106-852-69523, Contract: CT FP 80740-439-2020 (Colombian Ministry of Science, Technology, and Innovation — Minciencias), Grant IDs: CI-71242 (Universidad del Valle), 20 INTER 356 P2 (Universidad Autonoma de Occidente). Yves Dumont is (partially) supported by the DST/NRF SARChI Chair in Mathematical Models and Methods in Biosciences and Bioengineering at the University of Pretoria, South Africa (Grant 82770). Yves Dumont acknowledges the support of the *Conseil Régional de la Réunion* (France), the *Conseil Départemental de la Réunion* (France), the European Regional Development Fund (ERDF), and the *Centre de Coopération Internationale en Recherche Agronomique pour le Développement* (CIRAD), France. Yves Dumont also acknowledges partial funding from the ANR project BEEP (Behavioral Epidemiology and Evolution of Plant Pathogens - ANR-23-CE35-0012). Finally, the authors thank the support of the STIC AmSud program, through the project 23-STIC-02 BIO-CIVIP 'Biological control of insects vectors and insects pests'.

Appendix A. Proof of Propositions 2 and 3

Proof of Proposition 2. First, we compute the Jacobian related to system (7) with $\mathbf{\Phi}_1$ defined by (4) (see the equation in Box I), where $\mathbf{X} = (M, A, U)$. Thus, it is easy to compute that

$$J(\mathbf{E}_0) = \begin{pmatrix} -\mu & 0 & r\rho \\ 0 & -(\nu+\delta) & \eta + (1-r)\,\rho \\ 0 & \nu & -(\eta+\delta) \end{pmatrix},$$

and to show that the characteristic polynomial is given by

$$\begin{aligned} P_1^0(\lambda) &= -(\mu+\lambda)\Big[\lambda^2 + (\eta+\nu+2\delta)\lambda + (\eta+\delta)(\nu+\delta) - \big(\eta+(1-r)\rho\big)\nu\Big] \\ &= -(\mu+\lambda)\Big[\lambda^2 + (\nu+\eta+2\delta)\lambda + \delta(\nu+\eta+\delta) - (1-r)\rho\nu\Big] \\ &= -(\mu+\lambda)\Big[\lambda^2 + (\nu+\eta+2\delta)\lambda + \delta(\nu+\eta+\delta)\big(1-\mathcal{N}_F\big)\Big] \end{aligned}$$

When $\mathcal{N}_F < 1$, this polynomial has three roots with negative real parts meaning that $\mathbf{E}_0$ is LAS. Alternatively, $P_1^0(\lambda)$ has one root with positive real part when $\mathcal{N}_F > 1$ meaning that $\mathbf{E}_0$ is a saddle point (not a repeller). For example, a trajectory engendered by the initial condition $M(0) > 0, A(0) = 0, U(0) = 0$ converges to $\mathbf{E}_0$ even if $\mathcal{N}_F > 1$.

Let us now show that $\mathbf{E}_1^*$ is LAS when $\mathcal{N}_F > 1$. The Jacobian evaluated at $\mathbf{E}_1^*$ is

$$J\left(\mathbf{E}_1^*\right) = \begin{pmatrix} -\mu - \dfrac{r\rho}{\mathcal{N}_F}\sigma U_1^* & -\dfrac{r\rho}{\mathcal{N}_F}\sigma U_1^* & \dfrac{r\rho}{\mathcal{N}_F}\left(1-\sigma U_1^*\right) \\ -\dfrac{(1-r)\rho}{\mathcal{N}_F}\sigma U_1^* & -(\nu+\delta) - \dfrac{(1-r)\rho}{\mathcal{N}_F}\sigma U_1^* & \eta + \dfrac{(1-r)\rho}{\mathcal{N}_F}\left(1-\sigma U_1^*\right) \\ 0 & \nu & -(\eta+\delta) \end{pmatrix} \tag{A.1}$$

The characteristic polynomial of $J\left(\mathbf{E}_1^*\right)$ has the form

$$P_1^*(\lambda) = \lambda^3 + a_1\lambda^2 + a_2\lambda + a_3,$$

where $a_1 = -\mathrm{Tr}J\left(\mathbf{E}_1^*\right), a_3 = -\det J\left(\mathbf{E}_1^*\right)$, and

$$a_2 = \det\begin{vmatrix} J_{11} & J_{12} \\ J_{21} & J_{22} \end{vmatrix} + \det\begin{vmatrix} J_{11} & J_{13} \\ J_{31} & J_{33} \end{vmatrix} + \det\begin{vmatrix} J_{22} & J_{23} \\ J_{32} & J_{33} \end{vmatrix} := \Delta_1^{(1)} + \Delta_2^{(1)} + \Delta_3^{(1)} \tag{A.2}$$

with $J_{ij}, i, j = 1, 2, 3$ denoting the elements of (A.1). According to Routh–Hurwitz criterion (see, e.g., [59]), all roots of P_1^* have negative

$$J(\mathbf{X}) = \begin{pmatrix} J_{11} & J_{12} & J_{13} \\ J_{21} & J_{22} & J_{23} \\ J_{31} & J_{32} & J_{33} \end{pmatrix}$$

$$= \begin{pmatrix} -\mu - r\rho\sigma U e^{-\sigma(M+A+U)} & -r\rho\sigma U e^{-\sigma(M+A+U)} & r\rho(1-\sigma U)e^{-\sigma(M+A+U)} \\ -(1-r)\rho\sigma U e^{-\sigma(M+A+U)} & -(\nu+\delta)-(1-r)\rho\sigma U e^{-\sigma(M+A+U)} & \eta+(1-r)\rho(1-\sigma U)e^{-\sigma(M+A+U)} \\ 0 & \nu & -(\eta+\delta) \end{pmatrix},$$

Box I.

real parts if and only if the following conditions are satisfied:

$$a_1 > 0, \quad a_3 > 0, \quad \text{and} \quad a_1 a_2 - a_3 > 0. \tag{A.3}$$

Let us now check these conditions. First we note that

$$\mathrm{Tr} J\left(\mathbf{E}_1^*\right) = -\mu - \frac{r\rho}{\mathcal{N}_F}\sigma U_1^* - (\nu+\delta) - \frac{(1-r)\rho}{\mathcal{N}_F}\sigma U_1^* - (\eta+\delta) < 0,$$

and thus we have

$$a_1 = -\mathrm{Tr} J\left(\mathbf{E}_1^*\right) = \mu + \nu + \eta + 2\delta + \frac{\rho}{\mathcal{N}_F}\sigma U_1^* > 0. \tag{A.4}$$

To compute $\det J\left(\mathbf{E}_1^*\right)$, we observe that

$$\det J\left(\mathbf{E}_1^*\right) = -\nu\Delta_{32}^{(1)} - (\eta+\delta)\Delta_{33}^{(1)},$$

where $\Delta_{32}^{(1)}, \Delta_{33}^{(1)}$ are minors of $J\left(\mathbf{E}_1^*\right)$ obtained by elimination of the third row and either second or third column from (A.1). Effectively, we have

$$\begin{aligned}
\Delta_{32}^{(1)} &= -\left(\mu + \frac{r\rho}{\mathcal{N}_F}\sigma U_1^*\right) \times \left[\eta + \frac{(1-r)\rho}{\mathcal{N}_F}\left(1-\sigma U_1^*\right)\right] + \frac{(1-r)\rho}{\mathcal{N}_F}\sigma U_1^* \times \frac{r\rho}{\mathcal{N}_F}\left(1-\sigma U_1^*\right) \\
&= \mu\frac{(1-r)\rho}{\mathcal{N}_F}\sigma U_1^* - \eta\frac{r\rho}{\mathcal{N}_F}\sigma U_1^* - \mu\frac{(1-r)\rho}{\mathcal{N}_F} - \mu\eta, \\
\Delta_{33}^{(1)} &= \left(\mu + \frac{r\rho}{\mathcal{N}_F}\sigma U_1^*\right) \times \left[(\nu+\delta) + \frac{(1-r)\rho}{\mathcal{N}_F}\sigma U_1^*\right] - \frac{r\rho}{\mathcal{N}_F}\sigma U_1^* \times \frac{(1-r)\rho}{\mathcal{N}_F}\sigma U_1^* \\
&= \mu\frac{(1-r)\rho}{\mathcal{N}_F}\sigma U_1^* + (\nu+\delta)\frac{r\rho}{\mathcal{N}_F}\sigma U_1^* + \mu(\nu+\delta).
\end{aligned}$$

Then using the relationship

$$(\eta+\delta)(\nu+\delta) - \eta\nu = \delta(\delta+\eta+\nu) = \frac{(1-r)\rho\nu}{\mathcal{N}_F}, \tag{A.5}$$

we obtain

$$\begin{aligned}
\det J\left(\mathbf{E}_1^*\right) &= -\nu\left[\mu\frac{(1-r)\rho}{\mathcal{N}_F}\sigma U_1^* - \eta\frac{r\rho}{\mathcal{N}_F}\sigma U_1^* - \mu\frac{(1-r)\rho}{\mathcal{N}_F} - \mu\eta\right] \\
&\quad - (\eta+\delta)\left[\mu\frac{(1-r)\rho}{\mathcal{N}_F}\sigma U_1^* + (\nu+\delta)\frac{r\rho}{\mathcal{N}_F}\sigma U_1^* + \mu(\nu+\delta)\right] \\
&= -\mu(\nu+\eta+\delta)\frac{(1-r)\rho}{\mathcal{N}_F}\sigma U_1^* - \delta(\nu+\eta+\delta)\frac{r\rho}{\mathcal{N}_F}\sigma U_1^* \\
&\quad + \mu\frac{(1-r)\rho\nu}{\mathcal{N}_F} - \mu\delta(\nu+\eta+\delta) \\
&= -\left[(1-r)\mu + r\delta\right](\nu+\eta+\delta)\frac{\rho}{\mathcal{N}_F}\sigma U_1^* \\
&= -(\nu+\eta+\delta)\frac{\rho\vartheta}{\mathcal{N}_F}\sigma U_1^* < 0.
\end{aligned}$$

Thus, we have

$$a_3 = -\det J\left(\mathbf{E}_1^*\right) = \frac{\rho\vartheta}{\mathcal{N}_F}(\nu+\eta+\delta)\sigma U_1^* > 0. \tag{A.6}$$

To compute the coefficient a_2, we evaluate $\Delta_i^{(1)}, i = 1,2,3$ that appear in (A.2):

$$\begin{aligned}
\Delta_1^{(1)} &= \left(\mu + \frac{r\rho}{\mathcal{N}_F}\sigma U_1^*\right) \times \left(\nu + \delta + \frac{(1-r)\rho}{\mathcal{N}_F}\sigma U_1^*\right) - \frac{r\rho}{\mathcal{N}_F}\sigma U_1^* \times \frac{(1-r)\rho}{\mathcal{N}_F}\sigma U_1^* \\
&= \mu(\nu+\delta) + \mu\frac{(1-r)\rho}{\mathcal{N}_F}\sigma U_1^* + (\nu+\delta)\frac{r\rho}{\mathcal{N}_F}\sigma U_1^*, \\
\Delta_2^{(1)} &= (\eta+\delta)\left(\mu + \frac{r\rho}{\mathcal{N}_F}\sigma U_1^*\right), \\
\Delta_3^{(1)} &= (\eta+\delta)\left(\nu + \delta + \frac{(1-r)\rho}{\mathcal{N}_F}\sigma U_1^*\right) - \nu\left(\eta + \frac{(1-r)\rho}{\mathcal{N}_F}(1-\sigma U_1^*)\right)
\end{aligned}$$

Then according to (A.2) and using (A.5) we have

$$\begin{aligned}
a_2 &= \mu(\nu+\delta) + \mu(\eta+\delta) + (\eta+\delta)(\nu+\delta) - \eta\nu - \frac{(1-r)\rho\nu}{\mathcal{N}_F} \\
&\quad + \frac{\rho}{\mathcal{N}_F}\sigma U_1^*\left[(1-r)\mu + r(\nu+\delta) + r(\eta+\delta) + (1-r)(\eta+\delta) + (1-r)\nu\right] \\
&= \mu(\nu+\delta) + \mu(\eta+\delta) + (\vartheta+\nu+\eta+\delta)\frac{\rho}{\mathcal{N}_F}\sigma U_1^* > 0.
\end{aligned}$$

Our goal now is to show that $a_1 a_2 - a_3 > 0$. Before proceeding, we rewrite a_1 and a_2 in terms of a_3 using the formula (A.6):

$$a_1 = (\nu+\eta+\delta) + (\mu+\delta) + \frac{a_3}{\vartheta(\nu+\eta+\delta)}, \quad a_2 = \mu(\nu+\eta+2\delta) + \frac{a_3}{\nu+\eta+\delta} + \frac{a_3}{\vartheta},$$

so that

$$\begin{aligned}
a_1 a_2 - a_3 &= \left((\nu+\eta+\delta) + (\mu+\delta) + \frac{a_3}{\vartheta(\nu+\eta+\delta)}\right) \\
&\quad \times \left(\mu(\nu+\eta+2\delta) + \frac{a_3}{\vartheta} + \frac{a_3}{\nu+\eta+\delta}\right) - a_3 \\
&= (\nu+\eta+\delta)\left(\mu(\nu+\eta+2\delta) + \frac{a_3}{\vartheta}\right) + a_3 \\
&\quad + \left((\mu+\delta) + \frac{a_3}{\vartheta(\nu+\eta+\delta)}\right)\left(\mu(\nu+\eta+2\delta) + \frac{a_3}{\vartheta} + \frac{a_3}{\nu+\eta+\delta}\right) - a_3 \\
&= (\nu+\eta+\delta)\left(\mu(\nu+\eta+2\delta) + \frac{a_3}{\vartheta}\right) \\
&\quad + \left((\mu+\delta) + \frac{a_3}{\vartheta(\nu+\eta+\delta)}\right)\left(\mu(\nu+\eta+2\delta) + \frac{a_3}{\vartheta} + \frac{a_3}{\nu+\eta+\delta}\right) > 0.
\end{aligned}$$

Finally, the conditions (A.3) are satisfied and we conclude that $\mathbf{E}_1^*$ is LAS whenever $\mathcal{N}_F > 1$.

Proof of Proposition 3. The Jacobian related to the system (8) with $\mathbf{\Phi}_2$ defined by (5) is given by the equation in Box II where $\mathbf{X} = (M, A, U)$. Thus, it is easy to show that

$$J(\mathbf{E}_0) = \begin{pmatrix} -\mu & 0 & r\rho \\ -\gamma\nu & -\delta & \eta + (1-r)\rho \\ \gamma\nu & 0 & -\delta - \eta \end{pmatrix},$$

and to show that the characteristic polynomial is given by

$$\begin{aligned}
P_2^0(\lambda) &= -(\delta+\lambda)\left[\lambda^2 + (\delta+\eta+\mu)\lambda + (\delta+\eta)\mu - \gamma\nu\rho r\right] \\
&= -(\delta+\lambda)\left[\lambda^2 + (\delta+\eta+\mu)\lambda + (\delta+\eta)\mu\left(1-\mathcal{N}_M\right)\right]
\end{aligned}$$

When $\mathcal{N}_M < 1$, this polynomial has three roots with negative real parts meaning that $\mathbf{E}_0$ is LAS. Alternatively, $P_2^0(\lambda)$ has one root with positive real part when $\mathcal{N}_M > 1$ meaning that $\mathbf{E}_0$ is a saddle point (not a repeller). For example, a trajectory engendered by the initial condition $M(0) = 0, A(0) > 0, U(0) = 0$ converges to $\mathbf{E}_0$ even if $\mathcal{N}_M > 1$.

$$J(\mathbf{X}) = \begin{pmatrix} -\mu - r\rho\sigma U e^{-\sigma(A+M+U)} & -r\rho\sigma U e^{-\sigma(A+M+U)} & r\rho(1-\sigma U)e^{-\sigma(A+M+U)} \\ -\gamma\nu - (1-r)\rho\sigma U e^{-\sigma(A+M+U)} & -\delta - (1-r)\rho\sigma U e^{\sigma-(A+M+U)} & \eta + (1-r)\rho(1-\sigma U)e^{-\sigma(A+M+U)} \\ \gamma\nu & 0 & -(\eta+\delta) \end{pmatrix}$$

Box II.

Let us now show that $\mathbf{E}_2^*$ is LAS when $\mathcal{N}_M > 1$. We recall here that $U_2^* = \frac{\gamma\nu}{\eta+\delta} M_2^*$, and thus we have

$$J(\mathbf{E}_2^*) = \begin{pmatrix} -\mu(1+\sigma M_2^*) & -\mu\sigma M_2^* & \frac{r\rho}{\mathcal{N}_M} - \mu\sigma M_2^* \\ -\left(\gamma\nu + \frac{(1-r)}{r}\mu\sigma M_2^*\right) & -\left(\delta + \frac{(1-r)}{r}\mu\sigma M_2^*\right) & \eta + \frac{(1-r)\rho}{\mathcal{N}_M} - \frac{1-r}{r}\mu\sigma M_2^* \\ \gamma\nu & 0 & -(\eta+\delta) \end{pmatrix} \tag{A.7}$$

The characteristic polynomial of $J(\mathbf{E}_2^*)$ has the form

$$P_2^*(\lambda) = \lambda^3 + b_1\lambda^2 + b_2\lambda + b_3,$$

where $b_1 = -\mathrm{Tr}J(\mathbf{E}_2^*), b_3 = -\det J(\mathbf{E}_2^*)$, and

$$b_2 = \det\begin{vmatrix} J_{11} & J_{12} \\ J_{21} & J_{22} \end{vmatrix} + \det\begin{vmatrix} J_{11} & J_{13} \\ J_{31} & J_{33} \end{vmatrix} + \det\begin{vmatrix} J_{22} & J_{23} \\ J_{32} & J_{33} \end{vmatrix} := \Delta_1^{(2)} + \Delta_2^{(2)} + \Delta_3^{(2)} \tag{A.8}$$

with $J_{ij}, i, j = 1,2,3$ denoting the elements of (A.7). According to Routh–Hurwitz criterion (see, e.g., [59]), all roots of P_2^* have negative real parts if and only if the following conditions are satisfied:

$$b_1 > 0, \quad b_3 > 0, \quad \text{and} \quad b_1 b_2 - b_3 > 0. \tag{A.9}$$

Let us now check these conditions. First we note that

$$\mathrm{Tr}J(\mathbf{E}_2^*) = -2\delta - \eta - \mu(1+\sigma M_2^*) - \frac{(1-r)}{r}\mu\sigma M_2^* < 0,$$

and thus we have

$$b_1 = -\mathrm{Tr}J(\mathbf{E}_2^*) = \mu + \eta + 2\delta + \frac{\mu}{r}\sigma M_2^* > 0.$$

To compute $\det J(\mathbf{E}_2^*)$, we observe that

$$\det J(\mathbf{E}_2^*) = \gamma\nu\Delta_{31}^{(2)} - (\eta+\delta)\Delta_{33}^{(2)},$$

where $\Delta_{31}^{(2)}, \Delta_{33}^{(2)}$ are minors of $J(\mathbf{E}_2^*)$ obtained by elimination of the third row and either first or third column from (A.7). Effectively, we have

$$\begin{aligned} \Delta_{31}^{(2)} &= -\mu\sigma M_2^*\left(\eta + \frac{(1-r)\rho}{\mathcal{N}_M} - \frac{1-r}{r}\mu\sigma M_2^*\right) + \left(\frac{r\rho}{\mathcal{N}_M} - \mu\sigma M_2^*\right)\left(\delta + \frac{(1-r)}{r}\mu\sigma M_2^*\right) \\ &= -\eta\mu\sigma M_2^* - \delta\mu\sigma M_2^* + \delta\frac{r\rho}{\mathcal{N}_M} = -(\eta+\delta)\mu\sigma M_2^* + \frac{\mu\delta(\eta+\delta)}{\gamma\nu} \\ &= \mu(\eta+\delta)\left[\frac{\delta}{\gamma\nu} - \sigma M_2^*\right], \\ \Delta_{33}^{(2)} &= \mu(1+\sigma M_2^*)\left(\delta + \frac{(1-r)}{r}\mu\sigma M_2^*\right) - \mu\sigma M_2^*\left(\gamma\nu + \frac{(1-r)}{r}\mu\sigma M_2^*\right) \\ &= \delta\mu + \left(\delta + \mu\frac{(1-r)}{r}\right)\mu\sigma M_2^* - \gamma\nu\mu\sigma M_2^* \\ &= \delta\mu + \frac{\vartheta\mu}{r}\sigma M_2^* - \gamma\nu\mu\sigma M_2^*, \end{aligned}$$

and therefore

$$\begin{aligned} \det J(\mathbf{E}_2^*) &= \gamma\nu\mu(\eta+\delta)\left[\frac{\delta}{\gamma\nu} - \sigma M_2^*\right] - (\eta+\delta)\left[\delta\mu + \frac{\vartheta\mu}{r}\sigma M_2^* - \gamma\nu\mu\sigma M_2^*\right] \\ &= (\eta+\delta)\left[\delta\mu - \gamma\nu\mu\sigma M_2^* - \delta\mu - \frac{\vartheta}{r}\mu\sigma M_2^* + \gamma\nu\mu\sigma M_2^*\right] \\ &= -(\eta+\delta)\frac{\vartheta}{r}\mu\sigma M_2^* < 0 \end{aligned}$$

Thus we have

$$b_3 = -\det J(\mathbf{E}_2^*) = (\eta+\delta)\frac{\vartheta}{r}\mu\sigma M_2^* > 0 \tag{A.10}$$

To compute the coefficient b_2, we evaluate $\Delta_i^{(2)}, i = 1,2,3$ that appear in (A.8):

$$\begin{aligned} \Delta_1^{(2)} &= \Delta_{33}^{(2)} = \delta\mu + \frac{\vartheta\mu}{r}\sigma M_2^* - \gamma\nu\mu\sigma M_2^*, \\ \Delta_2^{(2)} &= (\eta+\delta)\mu(1+\sigma M_2^*) - \gamma\nu\left(\frac{r\rho}{\mathcal{N}_M} - \mu\sigma M_2^*\right) \\ &= (\eta+\delta)\mu(1+\sigma M_2^*) - \mu(\eta+\delta) + \gamma\nu\mu\sigma M_2^* \\ &= (\eta+\delta)\mu\sigma M_2^* + \gamma\nu\mu\sigma M_2^*, \\ \Delta_3^{(2)} &= (\eta+\delta)\left(\delta + \frac{(1-r)}{r}\mu\sigma M_2^*\right). \end{aligned}$$

Then using (A.8), we obtain

$$\begin{aligned} b_2 &= \delta\mu + \frac{\vartheta\mu}{r}\sigma M_2^* + (\eta+\delta)\mu\sigma M_2^* + \delta(\eta+\delta) + (\eta+\delta)\frac{(1-r)}{r}\mu\sigma M_2^* \\ &= \delta(\mu+\eta+\delta) + (\eta+\delta)\frac{1}{r}\mu\sigma M_2^* + \frac{\vartheta}{r}\mu\sigma M_2^* \\ &= \delta(\mu+\eta+\delta) + \frac{\eta+\delta+\vartheta}{r}\mu\sigma M_2^* > 0. \end{aligned}$$

Our goal now is to show that $b_1 b_2 - b_3 > 0$. Before proceeding, we rewrite b_1 and b_2 in terms of b_3 using the formula (A.10):

$$b_1 = (\mu+\delta) + (\eta+\delta) + \frac{b_3}{\vartheta(\eta+\delta)}, \qquad b_2 = \delta(\mu+\eta+\delta) + \frac{b_3}{\vartheta} + \frac{b_3}{\eta+\delta},$$

so that

$$\begin{aligned} b_1 b_2 - b_3 &= \left((\mu+\delta) + \frac{b_3}{\vartheta(\eta+\delta)} + (\eta+\delta)\right)\left(\delta(\mu+\eta+\delta) + \frac{b_3}{\vartheta} + \frac{b_3}{\eta+\delta}\right) - b_3 \\ &= (\eta+\delta)\left(\delta(\mu+\eta+\delta) + \frac{b_3}{\vartheta}\right) \\ &\quad + b_3 + \left((\mu+\delta) + \frac{b_3}{\vartheta(\eta+\delta)}\right)\left(\delta(\mu+\eta+\delta) + \frac{b_3}{\vartheta} + \frac{b_3}{\eta+\delta}\right) - b_3 \\ &= (\eta+\delta)\left(\delta(\mu+\eta+\delta) + \frac{b_3}{\vartheta}\right) \\ &\quad + \left((\mu+\delta) + \frac{b_3}{\vartheta(\eta+\delta)}\right)\left(\delta(\mu+\eta+\delta) + \frac{b_3}{\vartheta} + \frac{b_3}{\eta+\delta}\right) > 0. \end{aligned}$$

Finally, the conditions (A.9) are satisfied and we conclude that $\mathbf{E}_2^*$ is LAS whenever $\mathcal{N}_M > 1$.

Appendix B. Proof of Proposition 5

We have to solve the following algebraic system

$$\begin{cases} r\rho U e^{-\sigma(M+A+U)} - \alpha\dfrac{A_p}{A+A_p}M - \mu M = 0, & \text{(B.1a)} \\ (1-r)\rho U e^{-\sigma(M+A+U)} - \gamma\nu\dfrac{A}{A+A_p}M + \eta U - \delta A = 0, & \text{(B.1b)} \\ \gamma\nu\dfrac{A}{A+A_p}M - \eta U - \delta U = 0. & \text{(B.1c)} \end{cases}$$

From Eqs. (B.1a) and (B.1c), we obtain first

$$\rho U e^{-\sigma(M+A+U)} = \frac{1}{r}\left(\alpha\frac{A_p}{A+A_p}+\mu\right)M, \qquad U = \frac{\gamma\nu}{\eta+\delta}\,\frac{A}{A+A_p}M \tag{B.2}$$

and then using (B.1b), we arrive to

$$\left(\frac{1-r}{r}\left(\alpha\frac{A_p}{A+A_p}+\mu\right)-\gamma\nu\frac{A}{A+A_p}+\eta\frac{\gamma\nu}{\eta+\delta}\frac{A}{A+A_p}\right)M=\delta A.$$

The above expression can also be written as

$$\left((1-r)(\alpha+\mu)A_p+\left((1-r)\mu-\frac{\delta\gamma\nu r}{\eta+\delta}\right)A\right)M = r\delta\big(A+A_p\big)A.$$

Further, using the quantity θ_M, defined by (17), we arrive to

$$\left((1-r)(\alpha+\mu)A_p+\frac{\delta\gamma\nu r}{\eta+\delta}\big(\theta_M-1\big)A\right)M = r\delta\big(A+A_p\big)A.$$

Here, when $\theta_M > 1$, we have

$$M = \frac{r\delta\big(A+A_p\big)}{(1-r)(\alpha+\mu)A_p+\dfrac{\gamma r\nu\delta}{\eta+\delta}\big(\theta_M-1\big)A}A,$$

or

$$M = \frac{\eta+\delta}{\gamma\nu}\,\frac{A+A_p}{\dfrac{(\eta+\delta)(1-r)(\alpha+\mu)}{\gamma r\nu\delta}+\big(\theta_M-1\big)A}A \tag{B.3}$$

and

$$U = \frac{\gamma\nu}{\eta+\delta}\,\frac{A}{A+A_p}M = \frac{1}{\dfrac{(\eta+\delta)(1-r)(\alpha+\mu)}{\gamma r\nu\delta}A_p+\big(\theta_M-1\big)A}A^2. \tag{B.4}$$

Thus, M and U are now expressed in terms of A and the control parameters α, A_p. By plugging the above expressions for M and U into the left-hand side formula of (B.2), we obtain the following relationship

$$Ae^{-\sigma(M+A+U)} = \frac{1}{\rho r}\Big((\alpha+\mu)A_p+\mu A\Big)\frac{\eta+\delta}{\gamma\nu} = \frac{1}{\mu\mathcal{N}_M}\Big((\alpha+\mu)A_p+\mu A\Big).$$

Finally, replacing M and U in the exponential term leads to the following equation to solve

$$\mathcal{N}_M A f(A;A_p) - \frac{\alpha+\mu}{\mu}A_p = A, \tag{B.5}$$

where

$$f(A;A_p) := \exp\left(-\sigma\left(1+\frac{\delta r A_p+\delta r\left(\dfrac{\gamma\nu}{\eta+\delta}+1\right)A}{(1-r)(\alpha+\mu)A_p+\dfrac{\delta r\gamma\nu}{\eta+\delta}\big(\theta_M-1\big)A}\right)A\right),$$

which is a function of A also depending on the control parameter $A_p \geq 0$. Notably, when $A_p = 0$, we recover $f(A;0) = \dfrac{1}{\mathcal{N}_M}$. For the fixed values of α and A_p, let us denote the left-hand side of Eq. (B.5) by the function

$$\varphi(A;A_p) := \mathcal{N}_M A f(A;A_p) - \frac{\alpha+\mu}{\mu}A_p$$

that fulfills the condition $\varphi(0;A_p) < 0$ whenever $A_p > 0$. When $A > 0$, function $\varphi(A;A_p)$ increases first and then decreases. Therefore, depending on the value $A_p > 0$, there may exist two, one, or no solutions to Eq. (B.5) whose right-hand side is a straight line, see Fig. B.1. As shown in Fig. B.1, Eq. (B.5) has two solutions when A_p is relatively small. Then, by gradually increasing the value of A_p, one may get only one solution of (B.5). In such a case, the corresponding value of A_p will render the threshold value $A_p > A_p^{crit}$. Namely, Eq. (B.5) has no solution when $A_p > A_p^{crit}$ and no positive equilibria of the system (26) can exist for $A_p > A_p^{crit}$.

Thus, to identify the threshold value A_p^{crit} together with the underlying unique solution to Eq. (B.5), one must resolve the system of two equations:

$$\varphi(A;A_p) = A, \qquad \frac{\partial\varphi(A;A_p)}{\partial A} = 1. \tag{B.6}$$

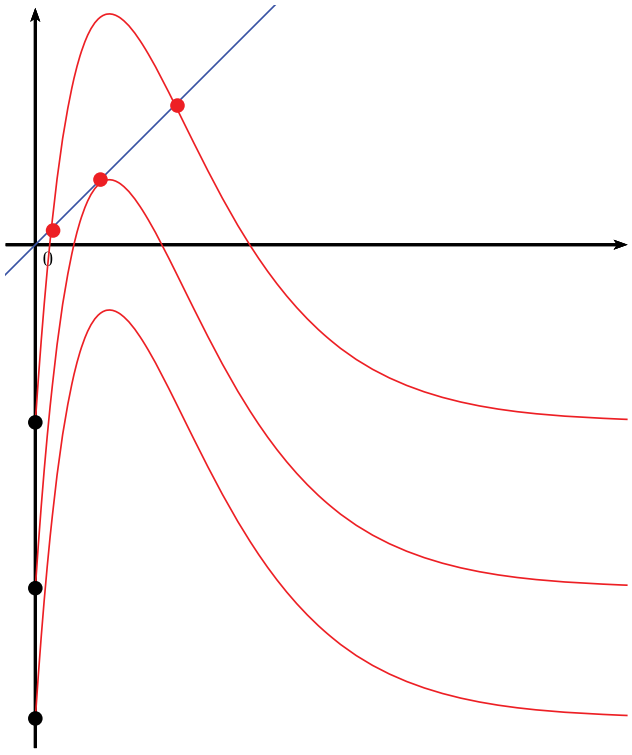

Fig. B.1. Possible intersections between $\varphi(A;A_p)$ (red color) and A (blue color) for different values of A_p.

Even though no analytical formula can be obtained for A_p^{crit}, its underlying value can be adequately approximated by solving the system (B.6) numerically. Also note that A_p^{crit} depends on $\alpha \in [0,1]$ as shown in Fig. 11, Section 5.

Furthermore, once A_p^{crit} is found as a solution of the nonlinear system (B.6), by setting $A_p < A_p^{crit}$ and plugging it into Eq. (B.5), we can obtain the coordinates $A_{1,p}^* < A_{2,p}^*, i = 1,2$ of the equilibria $\mathbf{E}_{i,p}^*, i = 1,2$ mentioned in the formulation of Proposition 5, while their coordinates $M_{i,p}^*$ and $U_{i,p}^*$ can be calculated using formulas (B.3) and (B.4) derived above for each $i = 1,2$. It is worthwhile to point out that Eq. (B.5) with $A_p > A_p^{crit}$ has no solution (see Fig. B.1).

Appendix C. Proof of Proposition 6

We will prove items (a) and (b) simultaneously, before proving item (c). But first, we show the existence of a threshold value, $\tilde{A}_p^{crit}$, such that: (i) no positive equilibrium exists when $A_p > \tilde{A}_p^{crit}$; (ii) one positive equilibrium, $\tilde{\mathbf{E}}_p^*$, exists when $A_p = \tilde{A}_p^{crit}$; (iii) two positive equilibria, $\tilde{\mathbf{E}}_{1,p}^*$ and $\tilde{\mathbf{E}}_{2,p}^*$, exist when $A_p < \tilde{A}_p^{crit}$.

Setting the first and third components of (28) equal to zero leads to

$$r\rho U = \left(\alpha\frac{A_p}{A+A_p}+\mu\right)Me^{\sigma M},$$

and, assuming $M > 0$,

$$r\rho\gamma\nu A-(\eta+\delta)\Big((\alpha+\mu)A_p+\mu A\Big)e^{\sigma M} = 0,$$

that is

$$\big(\mathcal{N}_M - e^{\sigma M}\big)A = \frac{\alpha+\mu}{\mu}A_p e^{\sigma M} \quad \Rightarrow \quad A = \frac{(\alpha+\mu)}{\mu\big(\mathcal{N}_M-e^{\sigma M}\big)}A_p e^{\sigma M}.$$

Setting the second component of (28) to zero and replacing A and U provides

$$r\rho\delta\frac{\alpha+\mu}{\mu}A_p = \big(\mathcal{N}_M-e^{\sigma M}\big)\Big((1-r)\rho+\eta\Big)\left(\alpha\frac{A_p}{A+A_p}+\mu\right)M$$

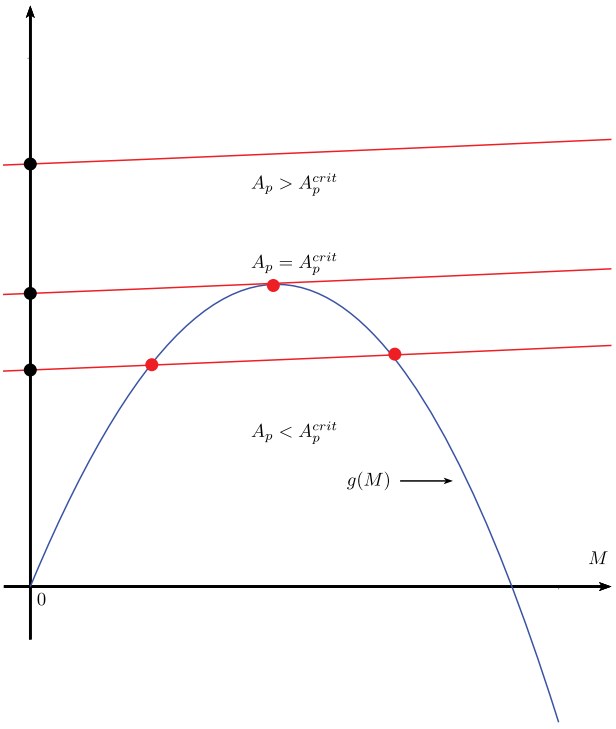

Fig. C.1. Possible intersections between $g(M)$ (blue color) and $h(M; A_p, \alpha)$ (red color) for different values of A_p.

$$= \left(\mathcal{N}_M - e^{\sigma M}\right)\Big((1-r)\rho + \eta\Big)\left(\alpha \frac{A_p}{\dfrac{\alpha+\mu}{\mu\left(\mathcal{N}_M - e^{\sigma M}\right)} A_p e^{\sigma M} + A_p} + \mu\right) M,$$

$$= \left(\mathcal{N}_M - e^{\sigma M}\right)\Big((1-r)\rho + \eta\Big)\mu \frac{(\alpha+\mu)\mathcal{N}_M}{\alpha e^{\sigma M} + \mu N_M} M.$$

From the above relationships, we have the following equation

$$\Big((1-r)\rho + \eta\Big)\mu\mathcal{N}_M M\left(\mathcal{N}_M - e^{\sigma M}\right) = r\rho\delta A_p\left(\mathcal{N}_M + \frac{\alpha}{\mu} e^{\sigma M}\right). \tag{C.1}$$

which can be viewed as $g_1(M) = g_2(M; A_p, \alpha)$, where

$$g(M) := \Big((1-r)\rho + \eta\Big)\mu\mathcal{N}_M M\left(\mathcal{N}_M - e^{\sigma M}\right) \quad \text{and}$$
$$h(M; A_p, \alpha) := r\rho\delta A_p\left(\mathcal{N}_M + \frac{\alpha}{\mu} e^{\sigma M}\right).$$

Here, the function $g(M)$ is increasing for small values of M and then decreasing as M becomes larger, so there exists $\widehat{M} > 0$ where g_1 attains a maximum $g\big(\widehat{M}\big)$. In its turn, the function $h(M; A_p, \alpha)$ is increasing for all $A_p > 0$ and $\alpha > 0$ (or constant when $\alpha = 0$). Thus, for any fixed $\alpha \in [0, 1]$ there exists a quantity $\tilde{A}_p^{crit} > 0$ such that Eq. (C.1) has: (a) no positive roots when $A_p > \tilde{A}_p^{crit}$; (b) two positive roots $M_{1,p}^*$ and $M_{2,p}^*$ when $A_p < \tilde{A}_p^{crit}$. Notably, when $A_p = \tilde{A}_p^{crit}$, the two positive roots collide ($M_{1,p}^* = M_{2,p}^*$) meaning that the auxiliary system (28) undergoes a pitchfork bifurcation. Fig. C.1 illustrates possible intersections between $g(M)$ (blue-colored curve) and $g(M; A_p, \alpha)$ (red-colored curves) for different values of A_p.

Now we prove (a), (b) and (c):

(a)–(b) Assume $A_p > \tilde{A}_p^{crit}$ and let $q \in \mathbb{R}_+$, with $q \geq q^* := \dfrac{\mu}{r\rho}\dfrac{\mathcal{N}_M}{\sigma}\ln \mathcal{N}_M$. We denote the right-hand side of the auxiliary system (28) by

$$\mathbf{H}(\mathbf{X}) := \begin{pmatrix} r\rho U e^{-\sigma M} - \alpha \dfrac{A_p}{A_p + A} M - \mu M \\ (1-r)\rho U + \eta U - \delta A \\ \nu \dfrac{\gamma M}{A_p + A} A - \eta U - \delta U \end{pmatrix},$$

where $\mathbf{X} = (M, A, U)$, and define

$$\mathbf{X}_q := \begin{pmatrix} \dfrac{r\rho}{\mu}\dfrac{1}{N_M} q \\ 2\dfrac{(1-r)\rho + \eta}{\delta} q \\ q \end{pmatrix}.$$

It is not difficult to check that $\mathbf{H}(\mathbf{E}_0) = \mathbf{E}_0$ and $\mathbf{H}(\mathbf{X}_q) \leq \mathbf{E}_0$, in a coordinate-wise sense. Let us also recall that the auxiliary system (28) is autonomous and cooperative. Then, according to Anguelov et al. (see Theorem 7 in [21]), we deduce that: (a) the auxiliary system (28) defines a positive dynamical system on $\mathbb{R}_+^3$; (b) $\mathbf{E}_0$ is GAS on $[\mathbf{E}_0, \mathbf{X}_q]$. Therefore, $\mathbf{E}_0$ is GAS on the set Ω, defined by (6), and also on $\mathbb{R}_+^3$ because Ω is an absorbing set (see Proposition 1).

(c) Assume $A_p < \tilde{A}_p^{crit}$. Let $\tilde{\mathbf{E}}_{1,p}^*$ and $\tilde{\mathbf{E}}_{2,p}^*$ be two equilibria such that $\tilde{\mathbf{E}}_{i,p}^* = \big(M_{i,p}^*, A_{i,p}^*, U_{i,p}^*\big)$, $i = 1, 2$, where $M_{1,p}^*$ and $M_{2,p}^*$ are positive roots of (C.1) that fulfill $M_{1,p}^* < M_{2,p}^*$ (in a coordinate-wise sense). Since A and U are increasing functions of M, we deduce that $\mathbf{E}_0 < \tilde{\mathbf{E}}_{1,p}^* < \tilde{\mathbf{E}}_{2,p}^*$. As it holds that $\mathbf{H}(\mathbf{X}_q) \leq \mathbf{E}_0 = \mathbf{H}(\tilde{\mathbf{E}}_{2,p}^*)$, by applying again Theorem 7 from [21], we conclude that $\tilde{\mathbf{E}}_{2,p}^*$ is GAS on $[\tilde{\mathbf{E}}_{2,p}^*, \mathbf{X}_q]$, that is, $\tilde{\mathbf{E}}_{2,p}^*$ is GAS on $\bigcup_{q \geq q^*}[\tilde{\mathbf{E}}_{2,p}^*, \mathbf{X}_q] = \left\{\mathbf{X} \in \mathbf{R}_+^3 : \ \mathbf{X} \geq \tilde{\mathbf{E}}_{2,p}^*\right\}$.
Finally, we deduce a similar result for $\mathbf{E}_0 < \tilde{\mathbf{E}}_{1,p}^*$, using Theorem 8 from [21], namely, all solutions initiated in $\left\{\mathbf{X} \in \mathbf{R}_+^3 : \ \mathbf{X} < \tilde{\mathbf{E}}_{1,p}^*\right\}$ converge to $\mathbf{E}_0$.

References

[1] O. Aidoo, P. Souza, P.A. da Silva, M. Picanço, R. Kyerematen, M. Sètamou, S. Ekesi, C. Borgemeister, Climate-induced range shifts of invasive species (*Diaphorina citri* Kuwayama), Pest. Manag. Sci. 78 (6) (2022) 2534–2549.

[2] E.E. Grafton-Cardwell, L.L. Stelinski, P.A. Stansly, Biology and management of Asian citrus psyllid, vector of the Huanglongbing pathogens, Annu. Rev. Entomol. 58 (1) (2013) 413–432.

[3] J.M. Bové, Huanglongbing: a destructive, newly-emerging, century-old disease of citrus, J. Plant Pathol. 88 (2006) 7–37.

[4] J.E. Angel, E.G. Hernandez, N.A. Herrera, L.Y. Gomez, A.P. Castro, A.M. Sepulveda, E.E. Ebratt, Citrus Huanglongbing: validation of real-time PCR (qPCR) for the detection of *Candidatus* Liberibacter asiaticus and *Candidatus* Liberibacter americanus in Colombia, Agron. Colomb. 32 (2014) 377–389.

[5] B. Reynaud, P. Turpin, F.M. Molinari, M. Grondin, S. Roque, F. Chiroleu, A. Fereres, H. Delatte, The African citrus psyllid *Trioza erytreae*: An efficient vector of *Candidatus Liberibacter asiaticus*, Front. Plant Sci. 13 (2022) 1089762.

[6] B. Aubert, S. Quilici, Biological control of the African and Asian citrus psyllids (Homoptera: Psylloidea) through eulophid and parasites (Hymenoptera: Chalcidoidea) in Reunion Island, in: International Organization of Citrus Virologists Conference Proceedings (1957-2010), vol. 9, no. 9, 1984, pp. 100–108.

[7] S.E. Halbert, C.A. Núñez, Distribution of the Asian citrus psyllid, *Diaphorina citri* Kuwayama (Rhynchota: Psyllidae) in the Caribbean basin, Fla. Èntomol. 87 (3) (2004) 401–402.

[8] E. Ebratt-Ravelo, L. Rubio-González, V. Costa, A. Castro-Ávila, E. Zambrano-Gómez, J. Ángel-Díaz, *Diaphorina citri* (Kuwayama, 1907) and *Tamarixia radiata* (Waterson, 1922) in citrus crops of Cundinamarca, Colombia, Agronomía Colomb. 29 (3) (2011) 487–493.

[9] A. Ramírez-Godoy, G. Puentes-Pérez, H. Restrepo-Díaz, Evaluation of the efficacy of neonicotinoid and pyrethroid insecticides in *Diaphorina citri* Kuwayama (Hemiptera: Liviidae) populations in Colombia, Rev. Colomb. de Cienc. HotíColas 12 (2) (2018) 358–368.

[10] A. Chow, M. Sétamou, Parasitism of *Diaphorina citri* (Hemiptera: Liviidae) by *Tamarixia radiata* (Hymenoptera: Eulophidae) on residential citrus in Texas: Importance of colony size and instar composition, Biol. Control 165 (2022) 104796.

[11] A. Garcia, A. Diniz, J. Parra, A fuzzy-based index to identify suitable areas for host-parasitoid interactions: Case study of the Asian citrus psyllid *Diaphorina citri* and its natural enemy *Tamarixia radiata*, Biol. Control 135 (2019) 135–140.

[12] T. Kondo, G. González, C. Tauber, Y.C. Guzmán, A.F. Vinasco, D. Forero, A checklist of natural enemies of *Diaphorina citri* Kuwayama (Hemiptera: Liviidae) in the department of Valle del Cauca, Colombia and the world, Insecta Mundi 0457 (2015).

[13] T. de Oliveira Portes, I. Pimentel, M. Zawadneak, Use and perspective of entomopathogenic fungi biocontrol agents of Asian citrus psyllid (*Diaphorina citri*): A bibliometric review, Res. Soc. Dev. 12 (12) (2023) e109121243984–e109121243984.

[14] M. Landa-Cadena, A. Trigos, F. Hernández-Rosas, A. Salinas-Castro, Identification of entomopathogenic fungi for the biological control of *Diaphorina citri* in citrus trees, Trop. Subtrop. Agroecosystems 28 (1) (2025).

[15] A. Levi-Zada, Pheromones and semiochemicals with potential use in management of citrus pests, Èntomol. Gen. 43 (4) (2023).

[16] H. Luo, X. Tang, Y. Deng, Z. Deng, M. Liu, The extraction and identification of active components of the sex pheromones of Asian citrus psyllid, *Diaphorina citri*, Pest. Biochem. Physiol. 192 (2023) 105421.

[17] M. Yalçın, Perspective chapter: Pheromone-based techniques in sustainable pest management, in: A. Habib (Ed.), Insecticides – Advances in Insect Control and Sustainable Pest Management, IntechOpen, London, UK, 2023.

[18] H. Volpe, M. Carmo-Sousa, R. Luvizotto, R. de Freitas, V. Esperança, J. Darolt, A. Pegoraro, D. Magalhães, A. Favaris, N. Wulff, M. Miranda, J. Bento, W. Leal, The greening-causing agent alters the behavioral and electrophysiological responses of the Asian citrus psyllid to a putative sex pheromone, Sci. Rep. 14 (1) (2024) 455.

[19] O.Z. Zanardi, H.X. Volpe, A.P. Favaris, W.D. Silva, R.A. Luvizotto, R.F. Magnani, V. Esperança, J.Y. Delfino, R. de Freitas, M.P. Miranda, J.R. Parra, J.M. Bento, W.S. Leal, Putative sex pheromone of the Asian citrus psyllid, *Diaphorina citri*, breaks down into an attractant, Sci. Rep. 8 (1) (2018) 455.

[20] M.D. Tapi, L. Bagny-Beilhe, Y. Dumont, Miridae control using sex-pheromone traps. Modeling, analysis and simulations, Nonlinear Anal. Real World Appl. 54 (2020) 103082.

[21] R. Anguelov, C. Dufourd, Y. Dumont, Mathematical model for pest-insect control using mating disruption and trapping, Appl. Math. Model. 52 (2017) 437–457.

[22] R.A. Taylor, E.A. Mordecai, C.A. Gilligan, J.R. Rohr, L.R. Johnson, Mathematical models are a powerful method to understand and control the spread of Huanglongbing, PeerJ 4 (2016) e2642.

[23] S. Gao, J. Guo, Y. Xu, Y. Tu, H. Zhu, Modeling and dynamics of physiological and behavioral resistance of Asian citrus psyllid, Math. Biosci. 340 (2021) 108674.

[24] I. Milosavljević, R. Amrich, V. Strode, M.S. Hoddle, Modeling the Phenology of Asian Citrus Psyllid (Hemiptera: Liviidae) in Urban Southern California: Effects of Environment, Habitat, and Natural Enemies, Environ. Èntomol. 47 (2) (2018) 233–243.

[25] A. Anzo Hernández, U.J. Giménez Mujica, C.A. Hernández Gracidas, J.J. Oliveros Oliveros, Optimizing control parameters for Huanglongbing disease in citrus orchards using SAIR-SI compartmental model, epidemic final size, and genetic algorithms, J. Math. Biol. 90 (1) (2025) 1–25.

[26] M.H. Ribeiro Luiz, L.T. Takahashi, R.C. Bassanezi, Optimal control in citrus diseases, Comput. Appl. Math. 40 (6) (2021) 191.

[27] F. Zhang, Z. Qiu, A. Huang, X. Zhao, Optimal control and cost-effectiveness analysis of a Huanglongbing model with comprehensive interventions, Appl. Math. Model. 90 (2021) 719–741.

[28] J. Ntahomvukiye, A. Temgoua, S. Bowong, Study of the population dynamics of *Busseola fusca*, maize pest, Acta Biotheor. 66 (2018) 379–397.

[29] D.G. Hall, Asian citrus psyllid life cycle and developmental biology, in: J. Qureshi, P. Stansly (Eds.), Asian Citrus Psyllid: Biology, Ecology and Management of the Huanglongbing Vector, CAB International, Boston MA, USA, 2020, pp. 1–11.

[30] P.-A. Bliman, D. Cardona-Salgado, Y. Dumont, O. Vasilieva, Implementation of control strategies for sterile insect techniques, Math. Biosci. 314 (2019) 43–60.

[31] E.J. Wenninger, D.G. Hall, Importance of multiple mating to female reproductive output in *Diaphorina citri*, Physiol. Entomol. 33 (4) (2008) 316–321.

[32] E. Wenninger, D.G. Hall, Daily timing of mating and age at reproductive maturity in *Diaphorina citri* (Hemiptera: Psyllidae), Fla. Èntomol. (2007) 715–722.

[33] H. Barclay, P. Van den Driessche, Pheromone trapping models for insect pest control, Res. Popul. Ecol. 25 (1) (1983) 105–115.

[34] U.K. Lubanga, R.A. Peters, M.J. Steinbauer, Convenience polyandry and the role of lone and reciprocal calls in a psyllid, Anim. Behav. 145 (2018) 1–10.

[35] R. Mankin, B. Rohde, Mating behavior of the Asian citrus psyllid, in: J. Qureshi, P. Stansly (Eds.), Asian Citrus Psyllid: Biology, Ecology and Management of the Huanglongbing Vector, CAB International, Boston MA, USA, 2020, pp. 30–42.

[36] L.A. Pérez, A.C. Busoli, P.A. Sotelo, A.M. Arcila, Biology and reproductive parameters of *Diaphorina citri* (Hemiptera: Liviidae) in different Rutaceae hosts, Rev. Colomb. de Entomología 43 (2) (2017) 141–150.

[37] A. Mwasunda, Modeling the impact of pheromone traps on the dynamics of fall armyworms: insights from maize biomass infestation, Model. Earth Syst. Environ. 11 (1) (2025) 26.

[38] M. di Bernardo, C. Budd, A. Champneys, P. Kowalczyk, A. Nordmark, G. Olivar-Tost, P. Piiroinen, Bifurcations in nonsmooth dynamical systems, SIAM Rev. 50 (4) (2008) 629–701.

[39] M. di Bernardo, A. Champneys, C. Budd, P. Kowalczyk, Qualitative theory of non-smooth dynamical systems, in: M. di Bernardo, A. Champneys, C. Budd, P. Kowalczyk (Eds.), Piecewise-Smooth Dynamical Systems: Theory and Applications, Springer, London, UK, 2008, pp. 47–119.

[40] D. Liberzon, Switching in systems and control, in: Systems & Control: Foundations & Applications, vol. 190, Birkhäuser, Boston, MA, USA, 2003.

[41] C. Barril, À. Calsina, J. Ripoll, A practical approach to R_0 in continuous-time ecological models, Math. Methods Appl. Sci. 41 (18) (2018) 8432–8445.

[42] H.-L. Li, X.-L. Zheng, Z.-Y. Huang, W. Lu, Review of reproductive behavior in *Diaphorina citri* (Kuwayama)(Homoptera: Liviidae), J. Plant Dis. Prot. 127 (2019) 601–606.

[43] D. Hall, An assessment of yellow sticky card traps as indicators of the abundance of adult *Diaphorina citri* (Hemiptera: Psyllidae) in citrus, J. Econ. Entomol. 102 (1) (2009) 446–452.

[44] I. Coutinho-Abreu, L. Forster, T. Guda, A. Ray, Odorants for surveillance and control of the Asian citrus psyllid (*Diaphorina citri*), PLoS One 9 (10) (2014) e109236.

[45] R. Mann, R. Rouseff, J. Smoot, N. Rao, W. Meyer, S. Lapointe, P. Robbins, D. Cha, C. Linn, F. Webster, S. Tiwari, L. Stelinski, Chemical and behavioral analysis of the cuticular hydrocarbons from Asian citrus psyllid, *Diaphorina citri*, Insect Sci. 20 (3) (2013) 367–378.

[46] R. Anguelov, Y. Dumont, I.V. Yatat Djeumen, Sustainable vector/pest control using the permanent sterile insect technique, Math. Methods Appl. Sci. 43 (18) (2020) 10391–10412.

[47] M. Kirkilionis, S. Walcher, On comparison systems for ordinary differential equations, J. Math. Anal. Appl. 299 (1) (2004) 157–173.

[48] P. van den Driessche, J. Watmough, Reproduction numbers and sub-threshold endemic equilibria for compartmental models of disease transmission, Math. Biosci. 180 (1–2) (2002) 29–48.

[49] C. Barril, A. Calsina, S. Cuadrado, J. Ripoll, On the basic reproduction number in continuously structured populations, Math. Methods Appl. Sci. 44 (1) (2021) 799–812.

[50] S. Marino, I.B. Hogue, C.R. Ray, D.E. Kirschner, A methodology for performing global uncertainty and sensitivity analysis in systems biology, J. Theoret. Biol. 254 (1) (2008) 178–196.

[51] G.R. Alves, A. Diniz, J. Parra, Biology of the Huanglongbing vector *Diaphorina citri* (Hemiptera: Liviidae) on different host plants, J. Econ. Entomol. 107 (2) (2014) 691–696.

[52] Y.H. Liu, J.H. Tsai, Effects of temperature on biology and life table parameters of the Asian citrus psyllid, *Diaphorina citri* Kuwayama (Homoptera: Psyllidae), Ann. Appl. Biol. 137 (3) (2000) 201–206.

[53] J.V. Shivankar, C.N. Rao, S. Singh, Studies on citrus psylla, *Diaphorina citri* Kuwayama : a review, Agricultural Reviews 21 (3) (2000) 199–204.

[54] R. Core Team, R: A Language and Environment for Statistical Computing, R Foundation for Statistical Computing, Vienna, Austria, 2022.

[55] L. Pedigo, G. Buntin, Handbook of Sampling Methods for Arthropods in Agriculture, CRC Press, Boca Raton, FL, USA, 1994.

[56] R.B. Matlock, J.B. Welch, F.D. Parker, Estimating population density per unit area from mark, release, recapture data, Ecol. Appl. 6 (4) (1996) 1241–1253.

[57] K.S. Onufrieva, A.V. Onufriev, How to count bugs: a method to estimate the most probable absolute population density and its statistical bounds from a single trap catch, Insects 12 (10) (2021) 932.

[58] P.-A. Bliman, M. De la Tousche, Y. Dumont, Feasibility and optimisation results for elimination by mass trapping in a metapopulation model, Appl. Math. Model. 144 (2025) 116047.

[59] J. Murray, Mathematical biology: I. An introduction, in: Interdisciplinary Applied Mathematics, vol. 17, Springer-Verlag, New York, USA, 2002.